

First Observation of $\bar{B} \rightarrow D^{(*)}\rho'^-, \rho'^- \rightarrow \omega\pi^-$

CLEO Collaboration

(March 9, 2001)

Abstract

We report on the observation of $\bar{B} \rightarrow D^*\pi^+\pi^-\pi^-\pi^0$ decays. The branching ratios for D^{*+} and D^{*0} are $(1.72 \pm 0.14 \pm 0.24)\%$ and $(1.80 \pm 0.24 \pm 0.27)\%$, respectively. Each final state has a $D^*\omega\pi^-$ component, with branching ratios $(0.29 \pm 0.03 \pm 0.04)\%$ and $(0.45 \pm 0.10 \pm 0.07)\%$ for the D^{*+} and D^{*0} modes, respectively. We also observe $\bar{B} \rightarrow D\omega\pi^-$ decays. The branching ratios for D^+ and D^0 are $(0.28 \pm 0.05 \pm 0.04)\%$ and $(0.41 \pm 0.07 \pm 0.06)\%$, respectively. A spin parity analysis of the $\omega\pi^-$ system in the $D\omega\pi^-$ final state shows a preference for a wide 1^- resonance. A fit to the $\omega\pi^-$ mass spectrum finds a central mass of $(1349 \pm 25_{-5}^{+10})$ MeV and width of $(547 \pm 86_{-45}^{+46})$ MeV. We identify this object as the $\rho(1450)$ or the ρ' .

J. P. Alexander,¹ C. Bebek,¹ B. E. Berger,¹ K. Berkelman,¹ F. Blanc,¹ V. Boisvert,¹
 D. G. Cassel,¹ P. S. Drell,¹ J. E. Duboscq,¹ K. M. Ecklund,¹ R. Ehrlich,¹ P. Gaidarev,¹
 L. Gibbons,¹ B. Gittelman,¹ S. W. Gray,¹ D. L. Hartill,¹ B. K. Heltsley,¹ L. Hsu,¹
 C. D. Jones,¹ J. Kandaswamy,¹ D. L. Kreinick,¹ M. Lohner,¹ A. Magerkurth,¹
 T. O. Meyer,¹ N. B. Mistry,¹ E. Nordberg,¹ M. Palmer,¹ J. R. Patterson,¹ D. Peterson,¹
 D. Riley,¹ A. Romano,¹ H. Schwarthoff,¹ J. G. Thayer,¹ D. Urner,¹ B. Valant-Spaight,¹
 G. Viehhauser,¹ A. Warburton,¹ P. Avery,² C. Prescott,² A. I. Rubiera,² H. Stoeck,²
 J. Yelton,² G. Brandenburg,³ A. Ershov,³ D. Y.-J. Kim,³ R. Wilson,³ T. Bergfeld,⁴
 B. I. Eisenstein,⁴ J. Ernst,⁴ G. E. Gladding,⁴ G. D. Gollin,⁴ R. M. Hans,⁴ E. Johnson,⁴
 I. Karliner,⁴ M. A. Marsh,⁴ C. Plager,⁴ C. Sedlack,⁴ M. Selen,⁴ J. J. Thaler,⁴ J. Williams,⁴
 K. W. Edwards,⁵ A. J. Sadoff,⁶ R. Ammar,⁷ A. Bean,⁷ D. Besson,⁷ X. Zhao,⁷ S. Anderson,⁸
 V. V. Frolov,⁸ Y. Kubota,⁸ S. J. Lee,⁸ R. Poling,⁸ A. Smith,⁸ C. J. Stepaniak,⁸ J. Urheim,⁸
 S. Ahmed,⁹ M. S. Alam,⁹ S. B. Athar,⁹ L. Jian,⁹ L. Ling,⁹ M. Saleem,⁹ S. Timm,⁹
 F. Wappler,⁹ A. Anastassov,¹⁰ E. Eckhart,¹⁰ K. K. Gan,¹⁰ C. Gwon,¹⁰ T. Hart,¹⁰
 K. Honscheid,¹⁰ D. Hufnagel,¹⁰ H. Kagan,¹⁰ R. Kass,¹⁰ T. K. Pedlar,¹⁰ J. B. Thayer,¹⁰
 E. von Toerne,¹⁰ M. M. Zoeller,¹⁰ S. J. Richichi,¹¹ H. Severini,¹¹ P. Skubic,¹¹ A. Undrus,¹¹
 V. Savinov,¹² S. Chen,¹³ J. W. Hinson,¹³ J. Lee,¹³ D. H. Miller,¹³ E. I. Shibata,¹³
 I. P. J. Shipsey,¹³ V. Pavlunin,¹³ D. Cronin-Hennessy,¹⁴ A.L. Lyon,¹⁴ E. H. Thorndike,¹⁴
 T. E. Coan,¹⁵ V. Fadeyev,¹⁵ Y. S. Gao,¹⁵ Y. Maravin,¹⁵ I. Narsky,¹⁵ R. Stroynowski,¹⁵
 J. Ye,¹⁵ T. Wlodek,¹⁵ M. Artuso,¹⁶ K. Benslama,¹⁶ C. Boulahouache,¹⁶ K. Bukin,¹⁶
 E. Dambasuren,¹⁶ G. Majumder,¹⁶ R. Mountain,¹⁶ T. Skwarnicki,¹⁶ S. Stone,¹⁶
 J.C. Wang,¹⁶ A. Wolf,¹⁶ S. Kopp,¹⁷ M. Kostin,¹⁷ A. H. Mahmood,¹⁸ S. E. Csorna,¹⁹
 I. Danko,¹⁹ K. W. McLean,¹⁹ Z. Xu,¹⁹ R. Godang,²⁰ G. Bonvicini,²¹ D. Cinabro,²¹
 M. Dubrovin,²¹ S. McGee,²¹ G. J. Zhou,²¹ A. Bornheim,²² E. Lipeles,²² S. P. Pappas,²²
 A. Shapiro,²² W. M. Sun,²² A. J. Weinstein,²² D. E. Jaffe,²³ R. Mahapatra,²³ G. Masek,²³
 H. P. Paar,²³ D. M. Asner,²⁴ A. Eppich,²⁴ T. S. Hill,²⁴ R. J. Morrison,²⁴ R. A. Briere,²⁵
 G. P. Chen,²⁵ T. Ferguson,²⁵ and H. Vogel²⁵

¹Cornell University, Ithaca, New York 14853

²University of Florida, Gainesville, Florida 32611

³Harvard University, Cambridge, Massachusetts 02138

⁴University of Illinois, Urbana-Champaign, Illinois 61801

⁵Carleton University, Ottawa, Ontario, Canada K1S 5B6

and the Institute of Particle Physics, Canada

⁶Ithaca College, Ithaca, New York 14850

⁷University of Kansas, Lawrence, Kansas 66045

⁸University of Minnesota, Minneapolis, Minnesota 55455

⁹State University of New York at Albany, Albany, New York 12222

¹⁰Ohio State University, Columbus, Ohio 43210

¹¹University of Oklahoma, Norman, Oklahoma 73019

¹²University of Pittsburgh, Pittsburgh, Pennsylvania 15260

¹³Purdue University, West Lafayette, Indiana 47907

¹⁴University of Rochester, Rochester, New York 14627

¹⁵Southern Methodist University, Dallas, Texas 75275

¹⁶Syracuse University, Syracuse, New York 13244

- ¹⁷University of Texas, Austin, Texas 78712
- ¹⁸University of Texas - Pan American, Edinburg, Texas 78539
- ¹⁹Vanderbilt University, Nashville, Tennessee 37235
- ²⁰Virginia Polytechnic Institute and State University, Blacksburg, Virginia 24061
- ²¹Wayne State University, Detroit, Michigan 48202
- ²²California Institute of Technology, Pasadena, California 91125
- ²³University of California, San Diego, La Jolla, California 92093
- ²⁴University of California, Santa Barbara, California 93106
- ²⁵Carnegie Mellon University, Pittsburgh, Pennsylvania 15213

I. INTRODUCTION

Currently most B meson decays are unknown. The decay width is comprised of hadronic decays, leptonic decays and semileptonic decays. Leptonic decays are predicted to be very small, $\approx 10^{-4}$ in branching fraction. The semileptonic branching ratio for $\bar{B} \rightarrow Xe^{-\nu}$, $X\mu^{-\nu}$, and $X\tau^{-\nu}$ totals approximately 25% [1]. The remainder must come from hadronic decays, where the measured exclusive branching ratios total only a small fraction of the hadronic width.

To be more explicit, the measured hadronic decay modes for the \bar{B}^0 including $D^+(n\pi^-)$, $D^{*+}(n\pi^-)$, where $3 \geq n \geq 1$, $D^{(*)}D_s^{-(*)}$, and J/ψ exclusive totals only about 10% [1]. The B^- modes total about 12%.

Yet, understanding hadronic decays of the B is crucial to ensuring that decay modes used for measurement of CP violation truly exhibit the underlying quark decay mechanisms expected theoretically.

It is also interesting to note that the average charged multiplicity in a hadronic B^0 decay is 5.8 ± 0.1 [2]. Since this multiplicity contains contributions from the decay of D^+ or D^{*+} normally present in \bar{B}^0 decay, we expect a sizeable, approximately several percent, decay rate into final states with four pions [3]. The seen $D^{(*)}(n\pi)^-$ final states for $n \leq 3$ are consistent with being quasi-two-body final states. For n of two the ρ^- dominates, while for n of three the a_1^- dominates [4]. These decays appear to occur from a simple spectator mechanism where the virtual W^- materializes as a single hadron: π^- , ρ^- or a_1^- . The decay rates can be understood in a simple ‘‘factorization’’ model where the decay rate is given by the product between two currents, one between the \bar{B} and the D and the other given by the virtual W^- transforming into the light hadron of interest [5].

In this paper we investigate final states for n of 4. We will show a large signal for the $D^{*+}\pi^+\pi^-\pi^-\pi^0$ final state in Section III. In Section IV we will show that a substantial fraction, $\sim 20\%$, arise from $D^{*+}\omega\pi^-$ decays and that the $\omega\pi^-$ mass distribution has a resonant structure around 1.4 GeV with a width of about 0.5 GeV. In Section V, similar conclusions are drawn about the $D^{*0}\pi^+\pi^-\pi^-\pi^0$ final state. The same structure is shown to exist in $D\omega\pi^-$ final states (Section VII) and we will use these events to show in Section VII F that the spin-parity is most likely 1^- . This state is identified as the ρ' , sometimes called the $\rho(1450)$. We perform a generalized Breit-Wigner fit to get the best values of the mass and width, discussed in Section IX and the Appendix.

Other resonant substructure is searched for, but not found (Section X). Finally we summarize our findings and compare with the predictions of factorization and other models in Section XI.

The data sample consists of 9.0 fb^{-1} of integrated luminosity taken with the CLEO II and II.V detectors [6] using the CESR e^+e^- storage ring on the peak of the $\Upsilon(4S)$ resonance and 4.4 fb^{-1} in the continuum at 60 MeV less center-of-mass energy. The sample contains 19.4 million B mesons.

II. COMMON SELECTION CRITERIA

Hadronic events are selected by requiring a minimum of five charged tracks, total visible energy greater than 15% of the center-of-mass energy, and a charged track vertex consistent with the nominal interaction point. To reject continuum we require that the Fox-Wolfram moment R_2 be less than 0.3 [7].

Track candidates are required to pass through a common spatial point defined by the origin of all tracks. Tracks with momentum below 900 MeV/c are required to have an ionization loss in the drift chamber within 3σ of that expected for their assigned mass.¹ (These requirements are not imposed on slow charged pions from D^{*+} decay.) Photon candidates are required to be in the “good barrel region,” within 45° of the plane perpendicular to the beam line that passes through the interaction point, and have an energy distribution in the CsI calorimeter consistent with that of an electromagnetic shower. To select π^0 's, we require that the diphoton invariant mass be between -3.0 to $+2.5\sigma$ of the π^0 mass, where σ varies with momentum and has an average value of approximately 5.5 MeV. The two-photon candidates are then kinematically fit by constraining their invariant mass be equal to the nominal π^0 mass.

We select D^0 and D^+ candidates via the decay modes shown in Table I. We require that the invariant mass of the D candidates lie within $\pm 2.5\sigma$ of the known D masses. The σ 's are also listed in Table I. The D^0 widths vary with the D^0 momentum, p , (units of MeV), while the D^+ widths are not momentum dependent.

We select D^{*+} candidates by imposing the addition requirement that the mass difference between π^+D^0 and D^0 combinations is within $\pm 2.5\sigma$ of the known mass difference. For the D^{*0} , we use the same requirement for the π^0D^0 decay. The mass difference resolutions are 0.63 and 0.90 MeV, for the π^+D^0 and π^0D^0 modes, respectively [8].

TABLE I. Mass Resolutions (σ) in MeV (p in units of MeV)

$D^+ \rightarrow K^- \pi^+ \pi^+$	$D^0 \rightarrow K^- \pi^+$	$D^0 \rightarrow K^- \pi^+ \pi^0$	$D^0 \rightarrow K^- \pi^+ \pi^+ \pi^-$
6.0	$p \times 0.93 \times 10^{-3} + 6.0$	$p \times 0.68 \times 10^{-3} + 11.6$	$p \times 0.92 \times 10^{-3} + 4.7$

III. OBSERVATION OF $\bar{B}^0 \rightarrow D^{*+} \pi^+ \pi^- \pi^- \pi^0$ DECAYS

A. \bar{B} Candidate Selection

We start by investigating the $D^{*+}(4\pi)^-$ final state.² The D^{*+} candidates are pooled with all combinations of $\pi^+ \pi^- \pi^- \pi^0$ mesons.

¹Here and throughout this paper σ indicates an r.m.s. error.

²In this paper $(4\pi)^-$ will always denote the specific combination $\pi^+ \pi^- \pi^- \pi^0$.

Next, we calculate the difference between the beam energy, E_{beam} , and the measured energy of the five particles, ΔE . The “beam constrained” invariant mass of the \overline{B} candidates, M_B , is computed from the formula

$$M_B^2 = E_{beam}^2 - \left(\sum_i \vec{p}_i \right)^2 \quad . \quad (1)$$

To further reduce backgrounds we define

$$\chi_b^2 = \left(\frac{\Delta M_{D^*}}{\sigma(\Delta M_{D^*})} \right)^2 + \left(\frac{\Delta M_D}{\sigma(\Delta M_D)} \right)^2 + \sum_{n(\pi^0)} \left(\frac{\Delta M_{\pi^0}}{\sigma(\Delta M_{\pi^0})} \right)^2 \quad , \quad (2)$$

where ΔM_{D^*} is the computed $D^* - D^0$ mass difference minus the nominal value, ΔM_D is the invariant candidate D^0 mass minus the known D^0 mass and ΔM_{π^0} is the measured $\gamma\gamma$ invariant mass minus the known π^0 mass. All π^0 's in the final state are included in the sum. The σ 's are the measurement errors. We select candidate events in each mode requiring that $\chi_b^2 < C_n$, where C_n varies for each decay D^0 decay mode. For the $Kn\pi$ decay modes we use $C_n = 12, 8,$ and $6,$ respectively.

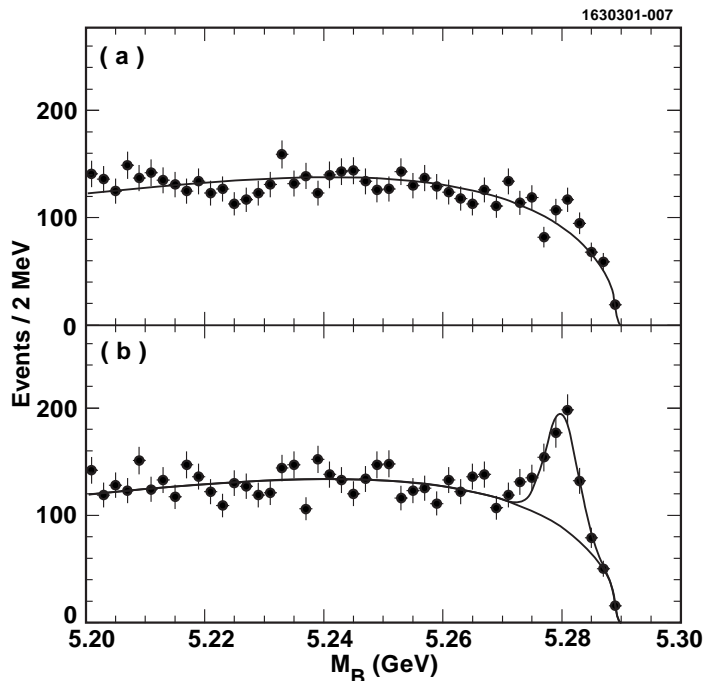


FIG. 1. The \overline{B} candidate mass spectra for the final state $D^{*+}\pi^+\pi^-\pi^-\pi^0$, with $D^0 \rightarrow K^-\pi^+$ (a) for ΔE sidebands and (b) for ΔE consistent with zero. The curve in (a) is a fit to the background distribution described in the text, while in (b) the shape from (a) is used with the normalization allowed to float and a signal Gaussian of width 2.7 MeV is added.

B. Branching Fraction and $(4\pi)^-$ Mass Spectrum

We start with the $D^0 \rightarrow K^-\pi^+$ decay mode. We show the candidate \overline{B} mass distribution, M_B , for ΔE in the side-bands from -5.0 to -3.0σ and 3.0 to 5.0σ on Fig. 1(a). The ΔE

resolution is 18 MeV (σ). The sidebands give a good representation of the background in the signal region. We fit this distribution with a shape given as

$$back(r) = p_1 r \sqrt{1 - r^2} e^{-p_2(1-r^2)} \quad , \quad (3)$$

where $r = M_B/5.2895$ GeV, and the p_i are parameters given by the fit.

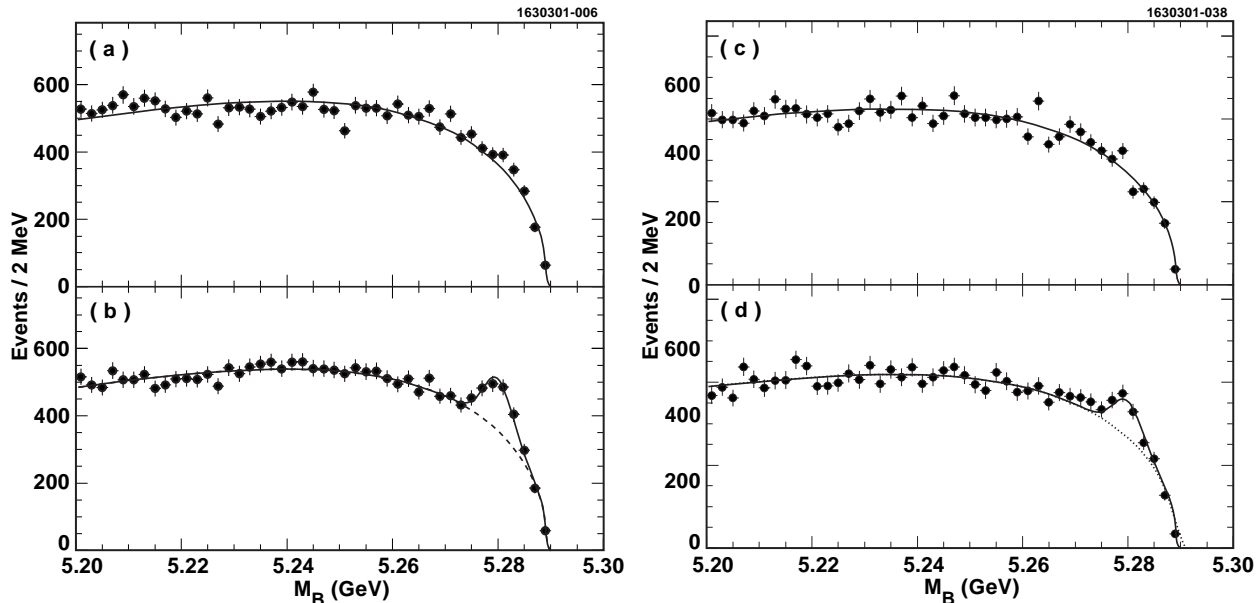


FIG. 2. The \overline{B} candidate mass spectra for the final state $D^{*+}\pi^+\pi^-\pi^-\pi^0$, the left-side plots are for $D^0 \rightarrow K^-\pi^+\pi^0$ (a) ΔE sidebands, (b) for ΔE consistent with zero; the right-side plots are for $D^0 \rightarrow K^-\pi^+\pi^+\pi^-$ (c) ΔE sidebands, (d) for ΔE consistent with zero. The curves in the top plots, (a) and (c), are fits to the background distribution described in the text, while in the bottom plots, (b) and (d), the shapes from (a) and (c) are used with the normalization allowed to float and a signal Gaussian of width 2.7 MeV is added.

We next view the M_B distribution for events having ΔE within 2σ around zero in Fig. 1(b). This distribution is fit with a Gaussian Signal function of width 2.7 MeV and the background function found above whose normalization is allowed to vary. The Gaussian signal width is found from Monte Carlo simulation. The largest and dominant component results from the energy spread of the beam. We find 358 ± 29 events in the signal peak.

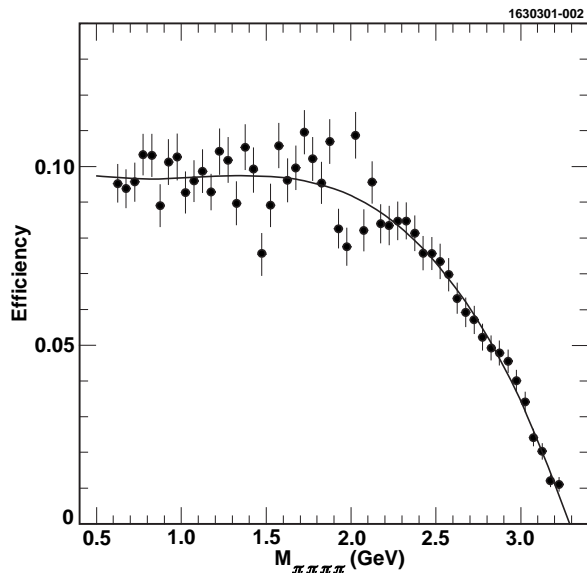
We repeat this procedure for the other two D^0 decay modes. The M_B spectrum for the ΔE sidebands and the signal region is shown in Fig. 2. The ΔE resolution is 22 MeV in the $K^-\pi^+\pi^0$ mode and 18 MeV in the $K^-\pi^+\pi^+\pi^-$ mode. Signal to background ratios are worse in these two modes, but the significance in both modes is quite large. The numbers of signal events are shown in Table II.

We choose to determine the branching fraction using only the $D^0 \rightarrow K^-\pi^+$ decay mode because of the relatively large backgrounds in the other modes and the decreased systematic error due to having fewer particles in the final state. In order to find the branching ratio we use the Monte Carlo generated efficiency, shown in Fig. 3 as a function of $(4\pi)^-$ mass. The efficiency falls off at larger $(4\pi)^-$ masses because the detection of the slow π^+ from the D^{*+} decay becomes increasingly more difficult. Since the efficiency varies with mass we need

TABLE II. Event numbers for the $D^{*+}\pi^+\pi^-\pi^-\pi^0$ final state

D^0 Decay Mode	Fitted # of events
$K^-\pi^+$	358 ± 29
$K^-\pi^+\pi^0$	543 ± 49
$K^-\pi^+\pi^+\pi^-$	329 ± 41

to determine the $(4\pi)^-$ mass spectrum. To rid ourselves of the problem of the background shape, we fit the \overline{B} candidate mass spectrum in 50 MeV bins of $(4\pi)^-$ mass. (The mass resolution is approximately 12 MeV.) The resulting $(4\pi)^-$ mass spectrum is shown in Fig. 4. There are indications of a low-mass structure around 1.4 GeV, that will be investigated further in this paper.


 FIG. 3. The efficiency for the final state $D^{*+}\pi^+\pi^-\pi^-\pi^0$, with $D^0 \rightarrow K^-\pi^+$.

We find

$$\mathcal{B}(\overline{B}^0 \rightarrow D^{*+}\pi^+\pi^+\pi^-\pi^0) = (1.72 \pm 0.14 \pm 0.24)\% \quad . \quad (4)$$

The systematic error arises mainly from our lack of knowledge about the tracking and π^0 efficiencies. We assign errors of $\pm 2.2\%$ on the efficiency of each charged track, $\pm 5\%$ for the slow pion from the D^{*+} , and $\pm 5.4\%$ for the π^0 . The error due to the background shape is evaluated in three ways. First of all, we change the background shape by varying the fitted parameters by 1σ . This results in a change of $\pm 3\%$. Secondly, we allow the shape, p_2 , to vary (the normalization, p_1 , was already allowed to vary). This results in 3.8% increase in the number of events. Finally, we choose a different background function

$$back'(r) = p_1 r \sqrt{1 - r^2} (1 + p_2 r + p_3 r^2 + p_4 r^3) \quad , \quad (5)$$

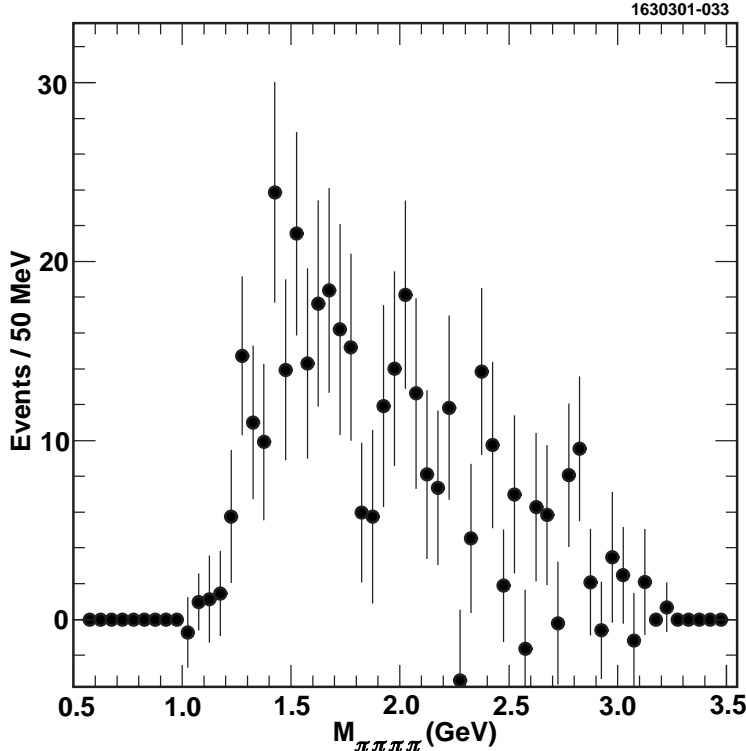


FIG. 4. The invariant mass spectra of $\pi^+\pi^-\pi^-\pi^0$ for the final state $D^{*+}\pi^+\pi^-\pi^-\pi^0$, with $D^0 \rightarrow K^-\pi^+$, found by fitting the \overline{B} yield in bins of 4π mass.

and repeat the fitting procedure. This results in a 3.7% decrease in the number of events. Taking a conservative estimate of the systematic error due to the background shape we arrive at $\pm 3.8\%$. We use the current particle data group values for the relevant D^{*+} and D^0 branching ratios of $(68.3 \pm 1.4)\%$ ($D^{*+} \rightarrow \pi^+ D^0$) and $(3.85 \pm 0.09)\%$ ($D^0 \rightarrow K^-\pi^+$), respectively [1]. The relative errors, 2.0% for the D^{*+} branching ratio and 2.3% for the D^0 are added in quadrature to the background shape error, the π^0 detection efficiency uncertainty and the tracking error. The total tracking error is found by adding the error in the charged particle track finding efficiency linearly for the 5 “fast” charged tracks and then in quadrature with the slow pion from the D^{*+} decay. The total systematic error is 14%.

We wish to search for narrow structures. However, we cannot fit the \overline{B} mass spectrum in small $(4\pi)^-$ mass intervals due to a lack of statistics. Thus we plot the $(4\pi)^-$ mass for events in the M_B peak for the $D^0 \rightarrow K^-\pi^+$ mode and the sum of all three modes in Fig. 5. We also plot two background samples: events at lower M_B (5.203 - 5.257 GeV) and those in the ΔE sideband separately. First we view the plots in the canonical 50 MeV bins. Both background distributions give a consistent if somewhat different estimates of the background shape. (Each background distribution has been normalized to the absolute number of background events as determined by the fit to the M_B distribution.) In any case no prominent narrow structures appear in the histograms for the 10 MeV binning.

The most accurate distribution of $4\pi^-$ mass is obtained by using the data in all three D^0 decay modes. The $4\pi^-$ mass distribution shown in Fig. 6 was found by fitting the M_B candidate mass distributions summed together. The distribution has been corrected for efficiency as a function of mass. There is an additional 14% systematic scale uncertainty on

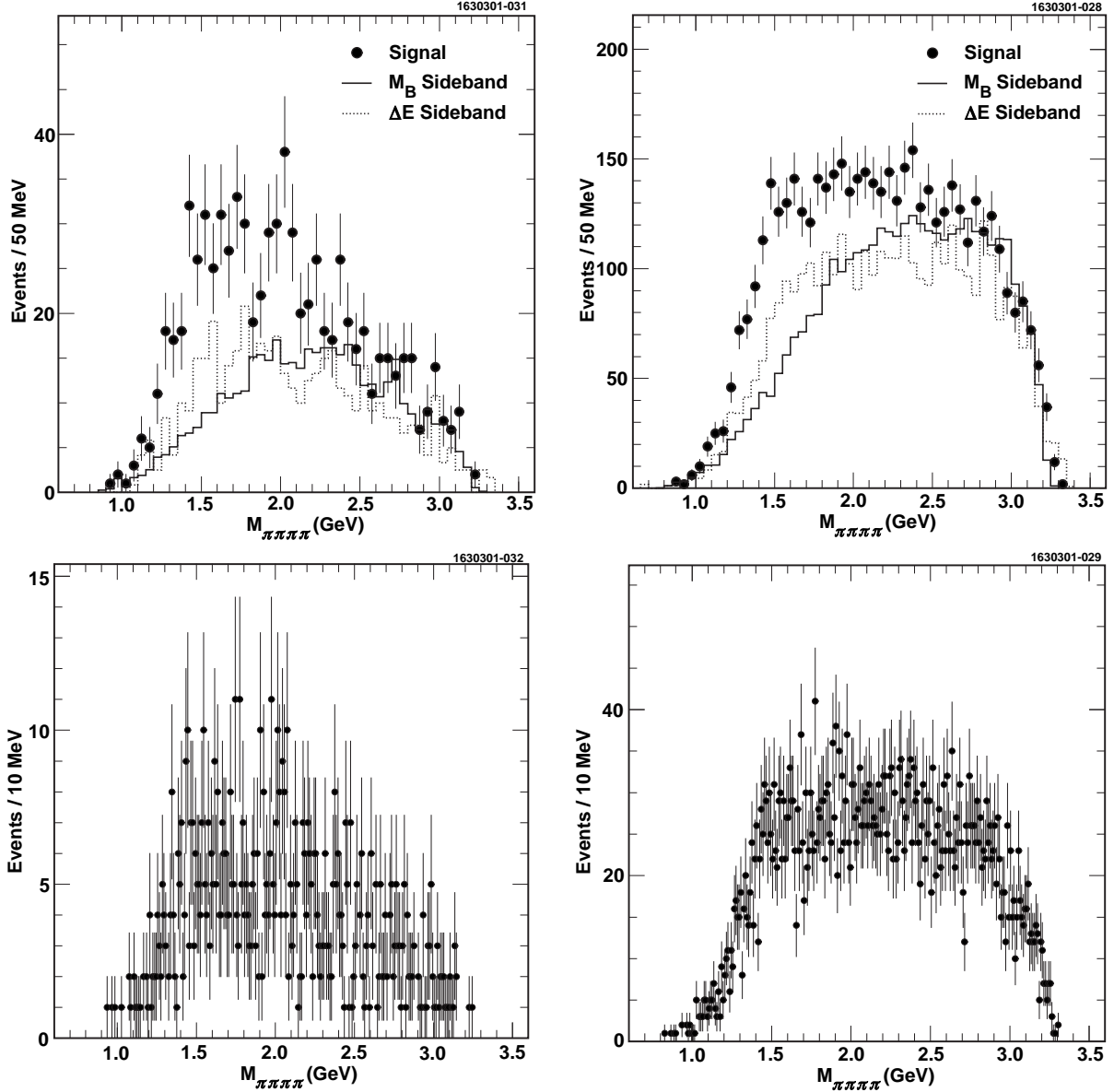


FIG. 5. The invariant mass spectra of $\pi^+\pi^-\pi^-\pi^0$ for the final state $D^{*+}\pi^+\pi^-\pi^-\pi^0$, with $D^0 \rightarrow K^-\pi^+$ (upper left), and the sum of all three D^0 decay modes (upper right). Events are selected by being within 2σ of the \overline{B} mass. The solid histogram is the background estimate from the M_B lower sideband and the dashed histogram is from the ΔE sidebands; both are normalized to the fitted number of background events. The same distributions in smaller bins (lower plots).

all the points.

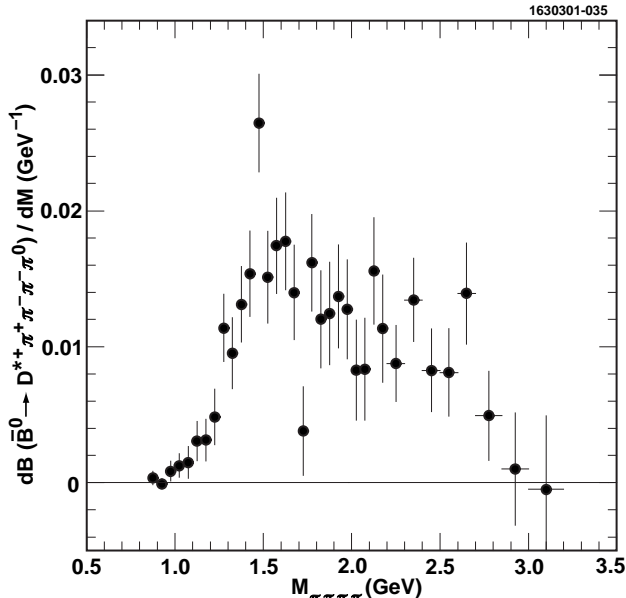


FIG. 6. The efficiency-corrected background-removed invariant mass spectra of $\pi^+\pi^-\pi^-\pi^0$ for the final state $D^{*+}\pi^+\pi^-\pi^-\pi^0$, for the sum of all three D^0 decay modes. (There is an additional scale uncertainty of 14%.)

IV. THE $\bar{B}^0 \rightarrow D^{*+}\omega\pi^-$ DECAY

To investigate the composition of the $(4\pi)^-$ final state, we now investigate the $\pi^+\pi^-\pi^0$ mass spectrum for the events in the \bar{B} peak. All three D^0 decay modes are used. We show the $\pi^+\pi^-\pi^0$ invariant mass distribution for events in the \bar{B} mass peak in Fig. 7 (there are two combinations per event). A clear signal is visible at the ω . The histograms on the figure are for events either in the lower M_B range, from 5.203 GeV to 5.257 GeV, or in the previously defined ΔE sidebands; no ω signal is visible.

The purity of the ω sample can be further improved by restricting candidates to certain regions of the Dalitz plot of the decay products. We define a cut on the Dalitz plot as follows. Let T_0 , T_+ and T_- be the kinetic energies of the pions, and Q be the difference between the ω mass, M_ω (equal to 782 MeV), and the mass of the 3 pions. We define two orthogonal coordinates X and Y , where

$$X = 3T_0/Q - 1 \quad (6)$$

$$Y = \sqrt{3}(T_+ - T_-)/Q \quad . \quad (7)$$

The kinematic limit that defines the Dalitz plot boundary is defined as

$$Y_{boundary}^2 = \frac{1}{3}(X_{boundary} + 1)(X_{boundary} + 1 + a)(1 + b/(X_{boundary} + 1 - c)) \quad (8)$$

where $a = 6m_0/Q$, $b = 6m^2/(M_\omega Q)$, $c = 3(M_\omega - m_0)^2/(2M_\omega Q)$, m is the mass of a charged pion and m_0 the mass of the neutral pion.

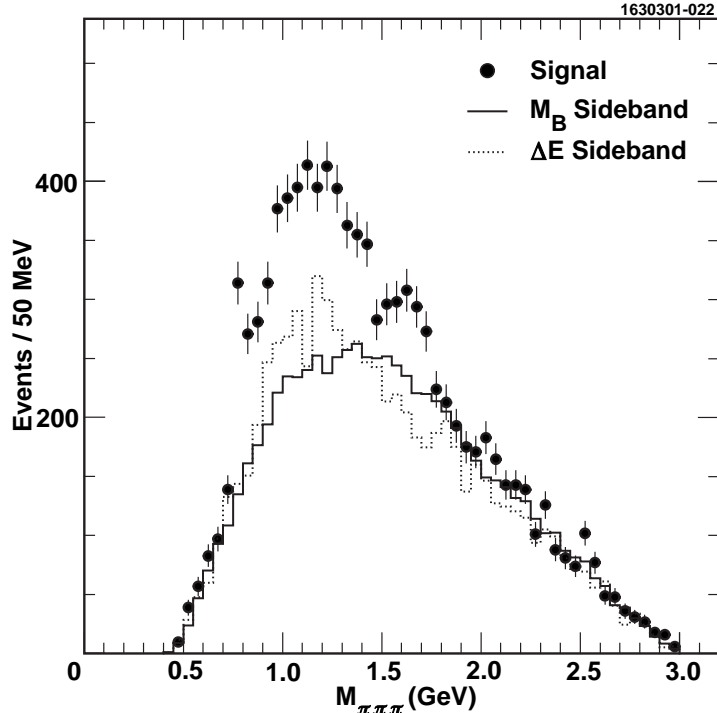


FIG. 7. The invariant mass spectra of $\pi^+\pi^-\pi^0$ for the final state $D^{*+}\pi^+\pi^-\pi^-\pi^0$ for all three D^0 decay modes. The solid histogram is the background estimate from the M_B lower sideband and the dashed histogram is from the ΔE sidebands; both are normalized to the fitted number of background events. (There are two mass combinations per event.)

For any set of three pion kinetic energies, we define a variable r , properly scaled to the kinematic limit as

$$r = \sqrt{\frac{X^2 + Y^2}{X_{boundary}^2 + Y_{boundary}^2}}, \quad (9)$$

where the boundary values are found by following the radial vector from (0,0) through (X,Y).

For events in the B mass peak we show in Fig. 8 the $\pi^+\pi^-\pi^0$ invariant mass for three different cuts on r . The ω signal is purified by restricting r , since the Dalitz plot density for a 1^- system decaying into $\pi^+\pi^-\pi^0$ peaks at r equals zero [9].

For further analysis we select ω candidates within the $\pi^+\pi^-\pi^0$ mass window of 782 ± 20 MeV with $r < 0.7$. We abandon the χ_b^2 cut here, as background is less of a problem. In Fig. 9 we show the \bar{B} candidate mass distribution for the $D^{*+}\omega\pi^-$ final state summing over all three D^0 decay modes. (The signal is fit with the same prescription as before.) There are 136 ± 15 events in the peak.

In Fig. 10 we show the $\omega\pi^-$ mass spectrum in the left-side plot. The solid histogram shows events from the lower M_B sideband region suitably normalized. The dotted histogram shows the background estimate from the ΔE sidebands, again normalized. In the signal distribution there is a wide structure around 1.4 GeV, that is inconsistent with background. We re-determine the $\omega\pi^-$ mass distribution by fitting the M_B distribution in bins of $\omega\pi^-$ mass, and this is shown on the right-side.

Knowing the $\omega\pi^-$ mass dependence of the efficiency we evaluate the branching fraction:

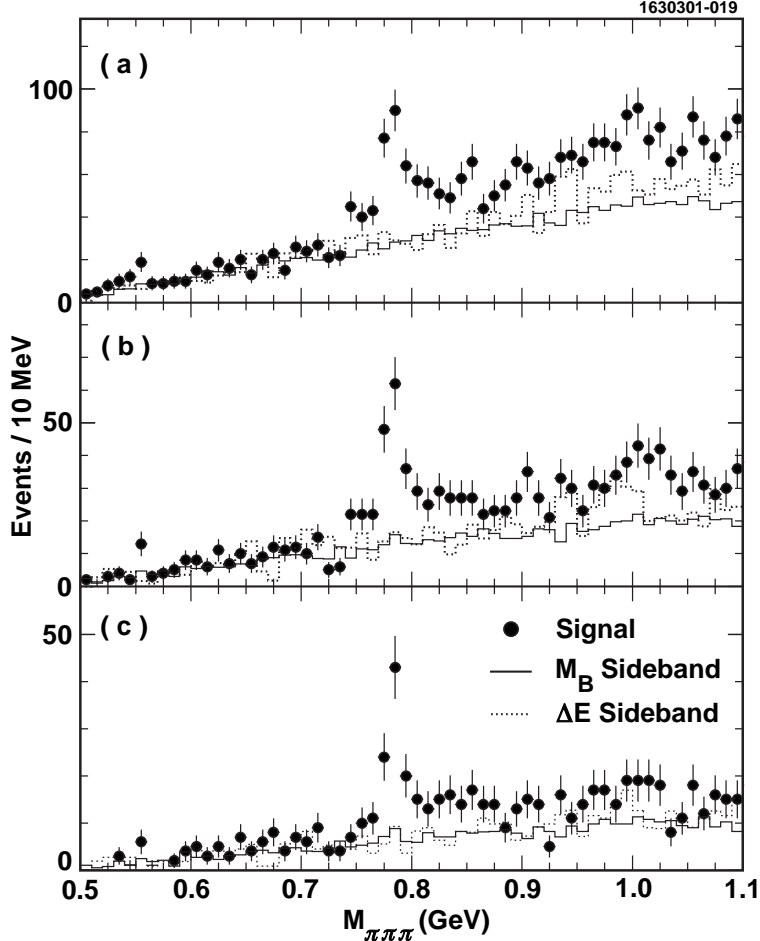


FIG. 8. The invariant mass spectra of $\pi^+\pi^-\pi^0$ for the final state $D^{*+}\pi^+\pi^-\pi^-\pi^0$ for all three D^0 decay modes for three selections on r less than: (a) 1, (b) 0.7 and (c) 0.5. The solid histogram is the background estimate from the M_B lower sideband and the dashed histogram is from the ΔE sidebands; both are normalized to the fitted number of background events.

$$\mathcal{B}(\bar{B}^0 \rightarrow D^{*+}\omega\pi^-) = (0.29 \pm 0.03 \pm 0.04)\% \quad . \quad (10)$$

We provisionally label the state at 1432 MeV the A^- and investigate its properties later. The $\omega\pi^-$ comprises about 17% of the $(4\pi)^-$ final state. All of the $\omega\pi^-$ final state is consistent with coming from A^- decay.

V. OBSERVATION OF $B^- \rightarrow D^{*0}\pi^+\pi^-\pi^-\pi^0$

We proceed in the same manner as for the \bar{B}^0 reaction with the exception that we use the $D^{*0} \rightarrow \pi^0 D^0$ decay mode and restrict ourselves to the $D^0 \rightarrow K^-\pi^+$ decay mode only due to large backgrounds in the other modes. The χ^2 is calculated according to equation 2 and we use a cut value of 8. The M_B distributions for ΔE sidebands and signal data are shown in Fig. 11 for the $D^0 \rightarrow K^-\pi^+$ decay mode. The ΔE resolution is 18 MeV. We see a signal of 195 ± 26 events yielding a branching fraction of

$$\mathcal{B}(B^- \rightarrow D^{*0}\pi^+\pi^-\pi^-\pi^0) = (1.80 \pm 0.24 \pm 0.27)\% \quad . \quad (11)$$

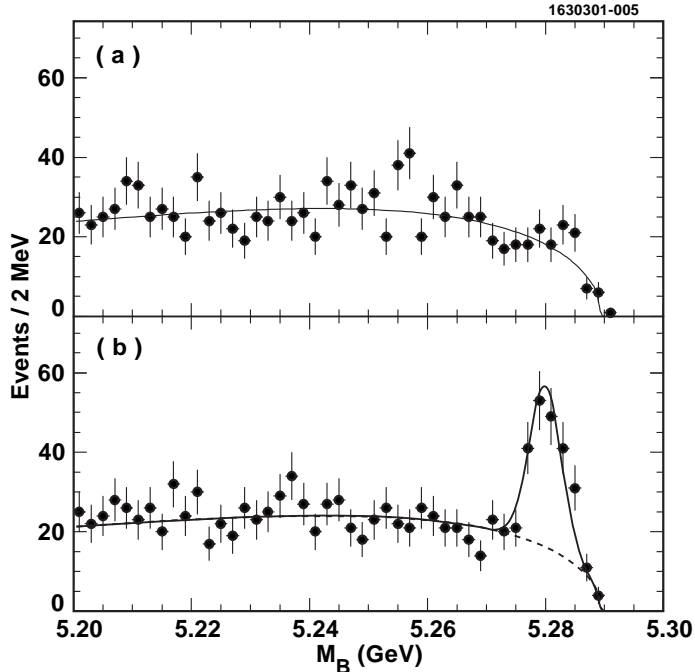


FIG. 9. The M_B spectra for $D^{*+}\omega\pi^-$ for all three D^0 decay modes. (a) ΔE sidebands and (b) ΔE around zero.

The $\pi^+\pi^-\pi^0$ mass spectrum shown in Fig. 12 shows the presence of an ω . Selecting on the presence of an ω with $r < 0.7$ we show the sideband and signal plots in Fig. 13. (Here we do not use the previously defined χ^2 cut.) The branching ratio, based on 26 ± 6 events is

$$\mathcal{B}(B^- \rightarrow D^{*0}\omega\pi^-) = (0.45 \pm 0.10 \pm 0.07)\% \quad . \quad (12)$$

In Fig. 14 we show the $\omega\pi^-$ mass spectrum. We see an enhancement at around 1.4 GeV as in the neutral \overline{B} case. (We do not have enough statistics here to fit the M_B distribution in bins of $\omega\pi^-$ mass.) The $\omega\pi^-$ fraction of the $(4\pi)^-$ final state is 25%, and all the $\omega\pi^-$ is consistent with coming from the A^- .

VI. ANALYSIS OF $D^{*+}\omega\pi^-$ DECAY ANGULAR DISTRIBUTIONS

The A^- is produced along with a spin-1 D^* from a spin-0 \overline{B} . If the A^- is spin-0 the D^* would be fully polarized in the $(J, J_z) = (1, 0)$ state. If the A^- were to be spin-1 any combinations of z-components would be allowed. It is natural then to examine the helicity angle of the D^{*+} by viewing the cosine of the helicity angle of the π^+ with respect to the \overline{B} in the D^{*+} rest frame.

Another decay angle that can be examined is that of the $\omega\pi$ system. If the A^- is spin-0, the ω is polarized in the $(1, 0)$ state and may be if the A^- is spin-1. Here the helicity angle is defined as the angle between the normal to the ω decay plane and the direction of the A^- in the ω rest frame. For a spin-0 A^- the distribution will be cosine-squared. Again

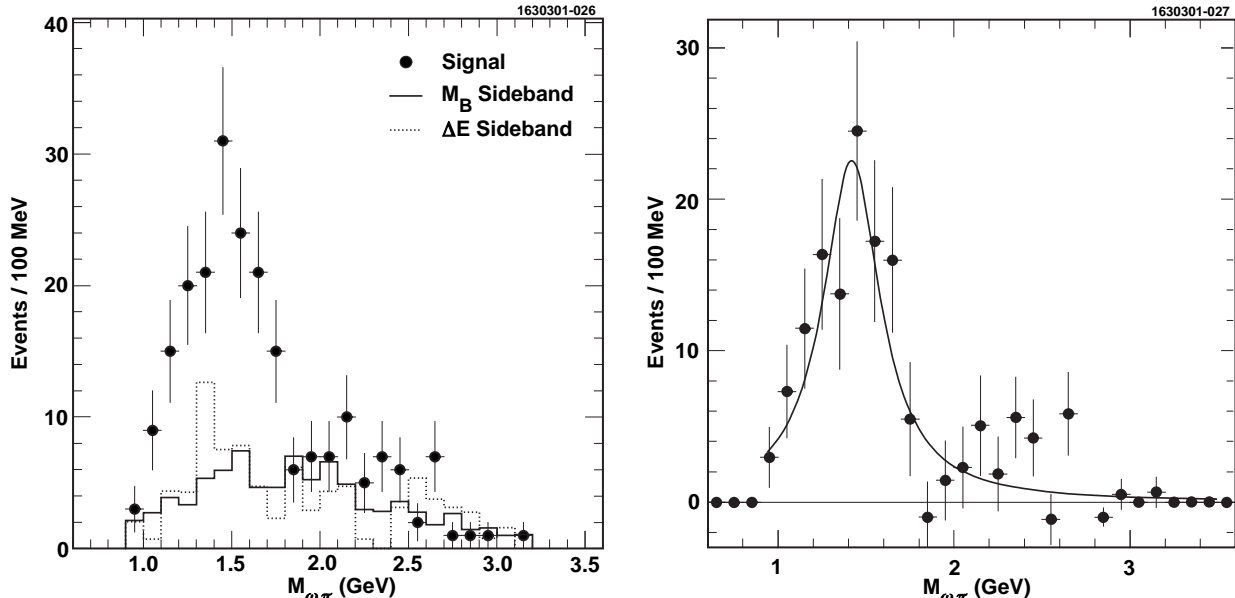


FIG. 10. The invariant mass spectra of $\omega\pi^-$ for the final state $D^{*+}\pi^+\pi^-\pi^-\pi^0$ for all three D^0 decay modes. (left) Signal events satisfy cuts on B mass, ΔE and ω mass (see text). The solid histogram is the background estimate from the M_B lower sideband and the dashed histogram is from the ΔE sidebands; both are normalized to the fitted number of background events. (right) The mass spectrum determined from fitting the M_B distribution and fit to a non-relativistic Breit-Wigner function that gives a mass of 1432 ± 37 MeV and a width of 376 ± 47 MeV.

full polarization is possible if the A^- is other than spin-0, but any distribution other than cosine-squared would demonstrate that the spin is not equal to zero.

For this analysis we use all three D^0 final states for the D^{*+} final state. To find the distributions we fit the number of events in the M_B candidate plot selected on different angle bins. The $\omega\pi$ mass is required to be between 1.1 and 1.9 GeV. This restriction leaves 111 ± 13 events.

In Fig. 15 we show the helicity angle distribution, $\cos\theta_{D^*}$ for the D^* decay. The data have been corrected for acceptance. We also show the expectation for spin-0 from the Monte Carlo. The data have been fit for the fraction of longitudinal polarization. We find

$$\frac{\Gamma_L}{\Gamma} = 0.63 \pm 0.09 \quad . \quad (13)$$

The systematic error is much smaller than the statistical error.

The $\cos\theta_{D^*}$ distribution is not consistent with full polarization, yielding a χ^2 of 17.7 for 5 degrees of freedom. The helicity angle distribution for the $A^- \rightarrow \omega\pi^-$, $\cos\theta_\omega$, is shown on Fig. 16. Furthermore the $\cos\theta_\omega$ distribution is quite inconsistent with a $\cos^2\theta_\omega$, yielding a χ^2 of 109 for 5 degrees of freedom. Therefore, we rule out a spin-0 assignment for the A^- .

To determine the J^P we need a more well defined final state. This is provided by analysis of $\overline{B} \rightarrow D\omega\pi^-$ decays.

VII. OBSERVATION OF $\overline{B} \rightarrow D\omega\pi^-$ DECAYS

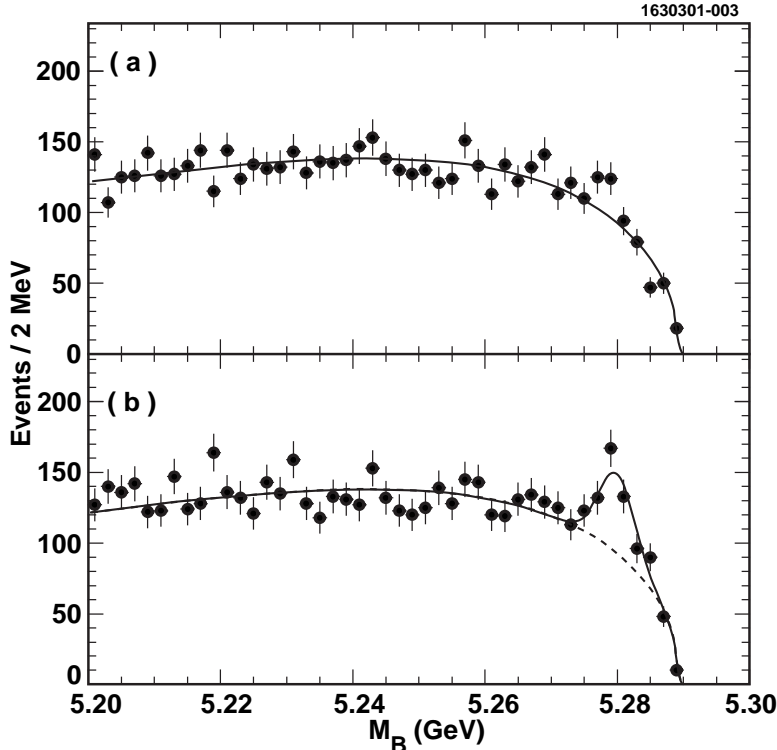


FIG. 11. The \bar{B} candidate mass spectra for the final state $D^{*0}\pi^+\pi^-\pi^-\pi^0$, with $D^0 \rightarrow K^-\pi^+$. Signal events satisfy cuts on B mass, ΔE and ω mass (see text). (a) for ΔE sidebands and (b) for ΔE consistent with zero. The curve in (a) is a fit to the background distribution described in the text, while in (b) the shape from (a) is used with the normalization allowed to float and a signal Gaussian of width 2.7 MeV is added.

A. \bar{B} candidate selection

Here we study the reactions $\bar{B} \rightarrow D\omega\pi^-$, with either a $D^0 \rightarrow K^-\pi^+$ or $D^+ \rightarrow K^-\pi^+\pi^+$ decay. Other D^0 or D^+ decays have substantially larger backgrounds.

Although we are restricting our search to ω 's, we define two $\pi^+\pi^-\pi^0$ samples. One within 20 MeV of the known ω mass (782 MeV) and the other in either low mass or high mass sideband defined as three π mass either between 732 and 752 MeV or between 812 and 832 MeV. We also require a cut on the ω Dalitz plot of $r < 0.7$.

To reduce backgrounds we define

$$\chi_b^2 = \left(\frac{\Delta M_D}{\sigma(\Delta M_D)} \right)^2 + \left(\frac{\Delta M_\omega}{\sigma(\Delta M_\omega)} \right)^2 + \left(\frac{\Delta M_{\pi^0}}{\sigma(\Delta M_{\pi^0})} \right)^2, \quad (14)$$

where ΔM_D is the invariant candidate D^0 mass minus the known D^0 mass, ΔM_ω is the invariant candidate ω mass minus the known ω mass, and ΔM_{π^0} is the measured $\gamma\gamma$ invariant mass minus the known π^0 mass. The σ 's are the measurement errors. We select candidate events requiring that χ_b^2 is < 12 for the $K\pi$ mode and < 6 for the $K\pi\pi$ mode.

B. $B^- \rightarrow D^0\omega\pi^-$ Signal

We start with the $D^0 \rightarrow K^-\pi^+$ decay mode, for events in the ω peak. We show the candidate \bar{B} mass distribution, M_B , for ΔE in the side-bands from -7.0 to -3.0σ and 7.0

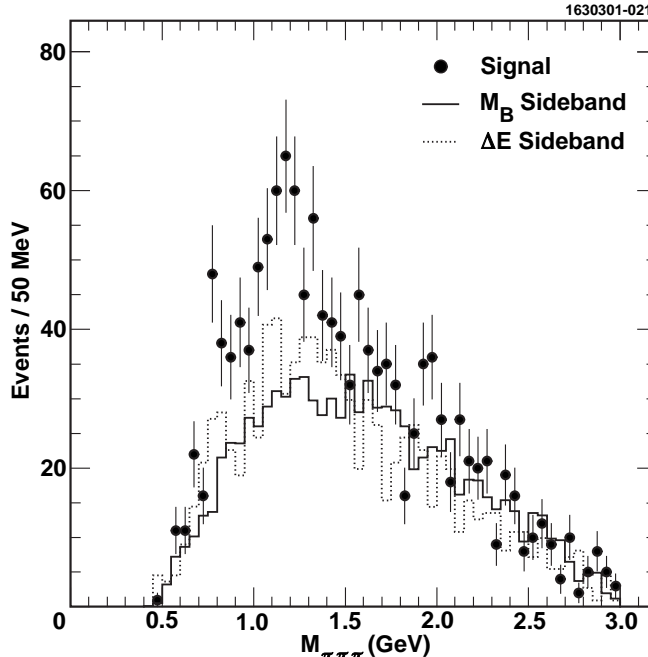


FIG. 12. The invariant mass spectra of $\pi^+\pi^-\pi^0$ for the final state $D^{*0}\pi^+\pi^-\pi^-\pi^0$ for the $D^0 \rightarrow K^-\pi^+$ decay mode. The solid histogram is the background estimate from the M_B lower sideband and the dashed histogram is from the ΔE sidebands; both are normalized to the fitted number of background events. There are two combinations per event.

to 3.0σ on Fig. 17(a). This gives a good representation of the background in the signal region. The ΔE resolution is 18 MeV (σ). We fit this distribution with the shape given in Equation 3.

We next view the M_B distribution for events having ΔE within 2σ around zero in Fig. 17(b). This distribution is fit with a Gaussian signal function of width 2.7 MeV and the background function found above whose normalization is allowed to vary. We find 88 ± 14 events in the signal peak.

We repeat this procedure for events in the ω sidebands. We use for our χ_b^2 definition pseudo- ω masses in the center of the sideband intervals. We show the M_B distribution for events in the ΔE sideband, defined above, and those having ΔE within 2σ around zero in Fig. 18. We find no significant signal.

C. $\bar{B}^0 \rightarrow D^+\omega\pi^-$ Signal

The same procedure followed for the D^0 final state is used for the D^+ final state. We show the candidate \bar{B} mass distribution, M_B , for events in the ΔE side-band on Fig. 19(a). The ΔE resolution is 18 MeV (σ). This gives a good representation of the background in the signal region. We fit this distribution with a shape given in equation 3.

We next view the M_B distribution for events having ΔE within 2σ around zero in Fig. 19(b). This distribution is fit with a Gaussian signal function of width 2.7 MeV and the background function found above whose normalization is allowed to vary. We find 91 ± 18

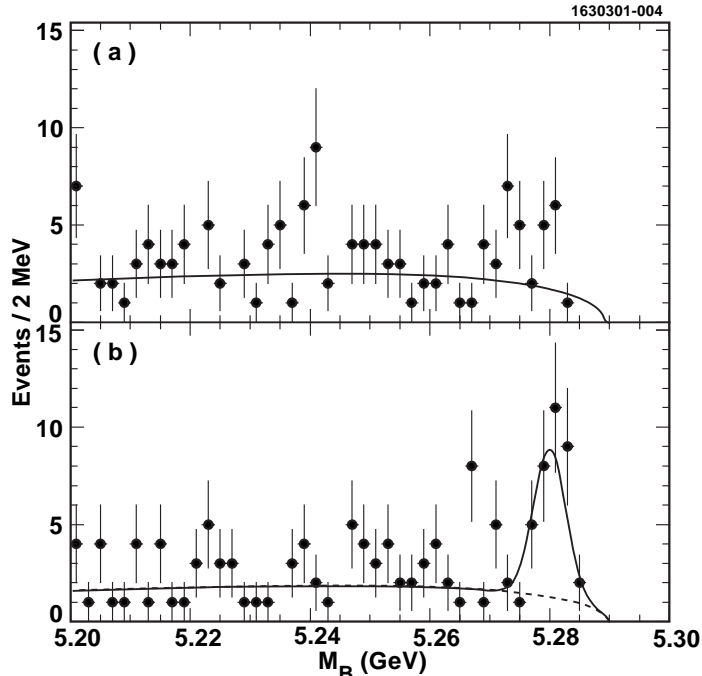


FIG. 13. The M_B spectra for $D^{*0}\omega\pi^-$ for the $D^0 \rightarrow K^-\pi^+$ decay mode. (a) ΔE sidebands and (b) ΔE around zero.

events in the signal peak.

We repeat this procedure for events in the ω sidebands. We show the M_B distribution for both ΔE sidebands and ΔE within 2σ around zero in Fig. 20.

There is no evidence of any signal in the ω sideband plot, leading to the conclusion that the signal is associated purely with ω .

D. Branching Fractions

We determine the branching ratios, shown in Table III, by performing a Monte Carlo simulation of the efficiencies in the two modes. We use the current particle data group values for the relevant ω , D^+ and D^0 branching ratios of $(88.8 \pm 0.7)\%$ ($\omega \rightarrow \pi^+\pi^-\pi^0$), $(9.0 \pm 0.6)\%$ ($D^+ \rightarrow K^-\pi^+\pi^+$) and $(3.85 \pm 0.09)\%$ ($D^0 \rightarrow K^-\pi^+$) [1]. The efficiencies listed in the table do not include these branching ratios [10].

TABLE III. Branching Fractions for the $D\omega\pi^-$ final state

D Decay Mode	Fitted # of events	Efficiency	Branching Fraction (%)
$K^-\pi^+$	88 ± 14	0.064	$0.41 \pm 0.07 \pm 0.06$
$K^-\pi^+\pi^+$	91 ± 18	0.046	$0.28 \pm 0.05 \pm 0.04$

The systematic error arises mainly from our lack of knowledge about the tracking and π^0 efficiencies. We assign errors of $\pm 2.2\%$ on the efficiency of each charged track, and $\pm 5.4\%$

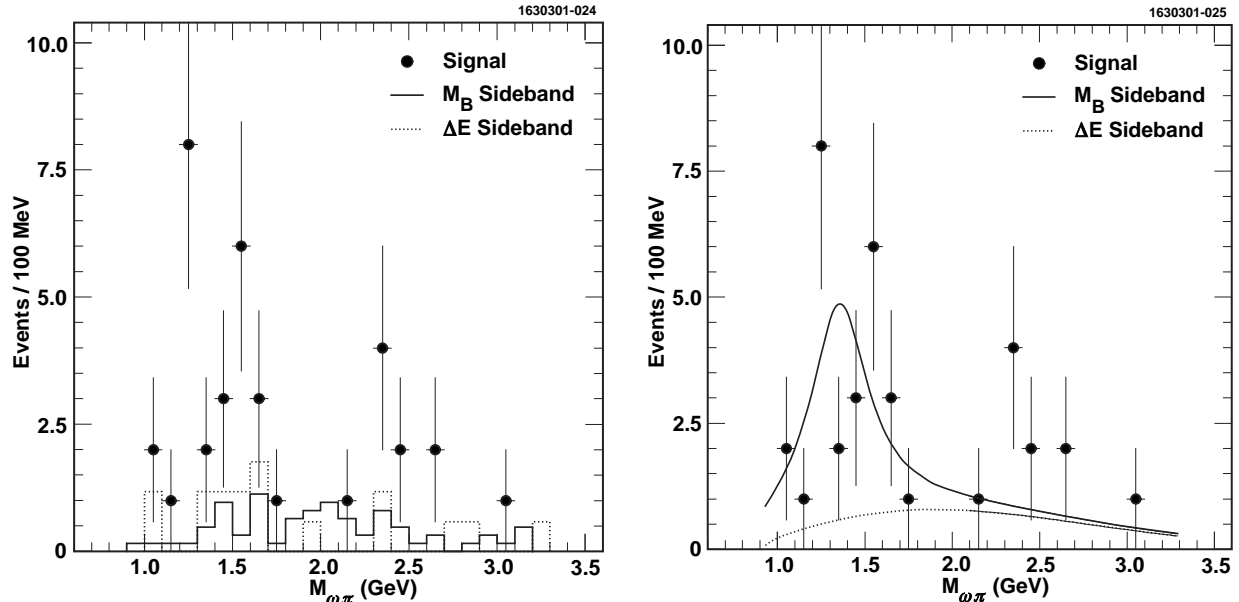


FIG. 14. The invariant mass spectra of $\omega\pi^-$ for the final state $D^{*0}\pi^+\pi^-\pi^-\pi^0$ for the $D^0 \rightarrow K^-\pi^+$ decay mode. (left) Signal events satisfy cuts on B mass, ΔE and ω mass (see text). The solid histogram is the background estimate from the M_B lower sideband and the dashed histogram is from the ΔE sidebands; both are normalized to the fitted number of background events. (right) The data fit to a non-relativistic Breit-Wigner signal and a smooth background function. The mass and width are 1367 ± 75 MeV and 439 ± 135 MeV, respectively.

for the π^0 . The error due to the background shape is evaluated in three ways. First of all, we change the background shape by varying the fitted parameters by 1σ . This results in a change of $\pm 5.0\%$. Secondly, we allow the shape, p_2 , to vary (the normalization, p_1 , was already allowed to vary). This results in 5.5% increase in the number of events. Finally, we choose a different background function given in equation 5 and repeat the fitting procedure. This results in a 1.0% decrease in the number of events. Taking a conservative estimate of the systematic error due to the background shape we arrive at $\pm 5.5\%$.

E. The $\omega\pi^-$ System

For all subsequent discussions we add the D^0 and D^+ final states together. We select sample of ω 's in the $\pi^+\pi^-\pi^0$ mass window of 782 ± 20 MeV using only combinations having $r < 0.7$ in the Dalitz plot.

In Fig. 21 we show the $\omega\pi^-$ mass spectrum in the left-side plot. The solid histogram shows events from the lower M_B sideband region (5.203 - 5.257 GeV) suitably normalized. The dotted histogram shows the background estimate from the ΔE sidebands, again normalized. In the signal distribution there is a wide structure around 1.4 GeV, that is inconsistent with background. We re-determine the $\omega\pi^-$ mass distribution by fitting the M_B distribution in bins of $\omega\pi^-$ mass, and this is shown on the right-side.

This structure appears identical to the one we observed in $\bar{B} \rightarrow D^*\omega\pi^-$ decays.

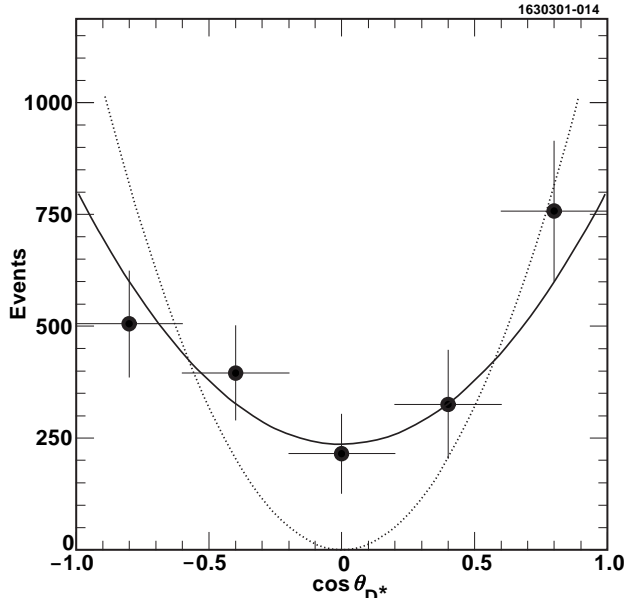


FIG. 15. The cosine of the angle between the D^0 and the D^* flight direction in the D^* rest frame for the D^*A^- final state (solid points) along with a fit (solid curve) allowing the amount of longitudinal and transverse polarization to vary. The dotted curve is the expectation for a spin-0 A^- .

F. Angular Distributions in $D\omega\pi^-$

We can determine the spin and parity of the A^- particle by studying the angular distributions characterizing its decay products. The decay chain that we are considering is $B \rightarrow A D$; $A \rightarrow \omega\pi$ and $\omega \rightarrow \pi^+\pi^-\pi^0$. The helicity formalism [11] is generally used in the analysis of these sequential decays. This formalism is well suited to relativistic problems involving particles with spin \vec{J} and momentum \vec{p} because the helicity operator $h = \vec{J} \cdot \vec{p}$ is invariant under both rotations and boosts along \hat{p} .

There are two relevant reference frames. The first one, that we will define $x_A y_A z_A$ is the rest frame of the A particle, with the \hat{z}_A axis pointing in the A direction of motion in the B rest frame. The \hat{x}_A direction is arbitrary. The second one, $x_\omega y_\omega z_\omega$, is related to $x_A y_A z_A$ by the rotation through 3 Euler angles $\phi_A, \theta_A, -\phi_A$, as shown in Fig. 22. The angle ϕ_A defines the orientation of the plane containing the ω direction in the A rest frame and the \hat{z}_A axis with respect to the $\hat{x}_A - \hat{z}_A$ plane. The angle θ_A is the polar angle of the ω momentum vector in the A rest frame. Note that the A decay plane has an azimuthal angle ϕ_A both in the $x_A y_A z_A$ and in the $x_\omega y_\omega z_\omega$ references. The angles θ_ω and ϕ_ω define the orientation of the ω decay plane in the ω rest frame. As the angle ϕ_A is arbitrary, the only angle that has a physical meaning is $\chi = \phi_A - \phi_\omega$, the opening angle between the A decay plane and the ω decay plane.

Both the \bar{B} meson and the D meson are pseudoscalar, therefore their helicity is 0. Thus A will be longitudinally polarized independently of its spin. In order to calculate the decay amplitude for this $A \rightarrow \omega\pi^-$ process, we need to sum over the ω helicity states:

$$\mathcal{A} = \sum_{\lambda_\omega} D_{0\lambda_\omega}^{*JA}(\phi_A, \theta_A, -\phi_A) D_{\lambda_\omega 0}^{*1}(\phi_\omega, \theta_\omega, -\phi_\omega) B_{\lambda_\omega 0}, \quad (15)$$

here $D_{0\lambda_\omega}^{*JA}(\phi_A, \theta_A, -\phi_A)$ is the rotation matrix that relates the $x_A y_A z_A$ and the $x_\omega y_\omega z_\omega$ frames

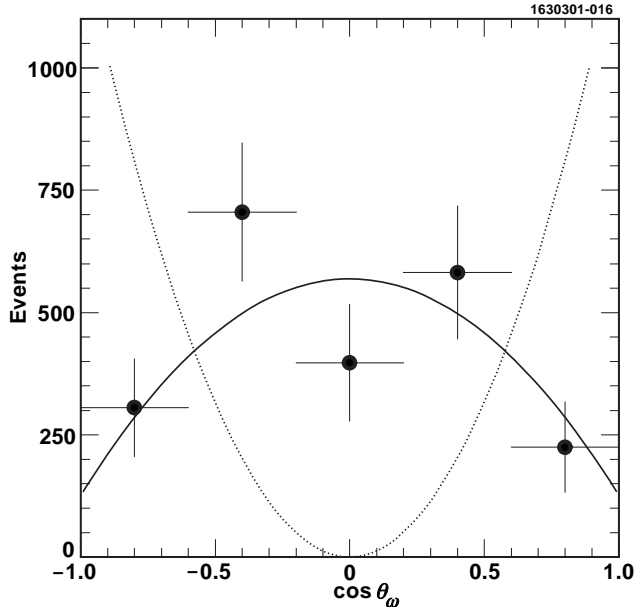


FIG. 16. The cosine of the angle between the normal to the $\pi^+\pi^-\pi^0$ decay plane and the ω boost direction for the D^*A^- final state (solid points) along with a fit (solid curve) allowing the amount of longitudinal and traverse polarization to vary. The dotted curve is the expectation for a spin-0 A^- .

and $D_{\lambda_{\omega 0}}^{*1}(\phi_{\omega}, \theta_{\omega}, -\phi_{\omega})$ is the rotation matrix relating the $x_{\omega}y_{\omega}z_{\omega}$ and the direction of the normal to the ω decay plane $\hat{n}(\theta_{\omega}, \phi_{\omega})$.

In general, there are three helicity amplitudes that contribute to this decay: B_{10} and B_{-10} , corresponding to a transverse ω polarization, and B_{00} , corresponding to a longitudinal ω polarization. This expression can be simplified by observing that $A \rightarrow \omega\pi$ is a strong decay and thus conserves parity. Thus, the helicity amplitudes are related as:

$$B_{10} = (-1)^{1-S(A)}\eta_A\eta_{\omega}\eta_{\pi}B_{-10}, \quad (16)$$

$$B_{00} = (-1)^{1-S(A)}\eta_A\eta_{\omega}\eta_{\pi}B_{00}. \quad (17)$$

where $S(A)$ is the spin of particle A and η_A, η_{ω} and η_{π} represent the intrinsic parity of the decaying particle and its decay products, respectively.

Eq. 16 relates the two transverse helicity amplitudes, while Eq. 17 forbids the presence of a longitudinal component under certain conditions. For example, if A is a 1^- object, the ω has transverse polarization and $B_{-10} = -B_{10}$. When the sign in Eqs. 16-17 is positive, two parameters determined by the hadronic matrix element affect the angular distribution and thus we cannot fully determine it only on the basis of our assumptions on the A spin parity. We have carried out the calculation of the predicted angular distributions including spin assignment for A up to 2. The predicted angular distributions are summarized in Table IV.

The statistical accuracy of our data sample is not sufficient to do a simultaneous fit of the joint angular distributions shown above. Thus only the projections along the $\theta_A, \theta_{\omega}$ and

TABLE IV. Differential angular distributions (modulo a proportionality constant) predicted for different spin assignments. (Note 0^+ is forbidden by parity conservation.)

J^P	$d\sigma/d\cos\theta_A d\cos\theta_\omega d\chi$
0^-	$ B_{00} ^2 \cos^2 \theta_\omega$
1^-	$ B_{10} ^2 \sin^2 \theta_A \sin^2 \theta_\omega \sin^2 \chi$
1^+	$ B_{10} ^2 \sin^2 \theta_A \sin^2 \theta_\omega^2 \cos^2 \chi^2 + B_{00} ^2 \cos^2 \theta_A \cos^2 \theta_\omega$ $- 1/2 \text{Re}(B_{10} B_{00}^*) \sin 2\theta_A \sin 2\theta_\omega \cos \chi$
2^-	$3 B_{10} ^2 \sin^2 2\theta_A \sin^2 \theta_\omega \cos^2 \chi + B_{00} ^2 (3 \cos^2 \theta_A - 1)^2 \cos^2 \theta_\omega$ $- \sqrt{3} \text{Re}(B_{10} B_{00}^*) \sin 2\theta_A (3 \cos^2 \theta_A - 1) \sin 2\theta_\omega \cos \chi$
2^+	$3/4 B_{10} ^2 \sin^2 2\theta_A \sin^2 \theta_\omega \sin^2 \chi$

TABLE V. Projection of the angular distributions along the $\cos\theta_A$, $\cos\theta_\omega$ and χ axes.

J^P	$d\sigma/d\cos\theta_A$	$d\sigma/d\cos\theta_\omega$	$d\sigma/d\chi$
0^-	$\frac{4\pi}{3} B_{00} ^2$	$4\pi B_{00} ^2 \cos^2 \theta_\omega$	$4/3 B_{00} ^2$
1^-	$\frac{4\pi}{3} B_{10} ^2 \sin^2 \theta_A$	$\frac{4\pi}{3} B_{10} ^2 \sin^2 \theta_\omega$	$\frac{8}{9} B_{10} ^2 \sin^2 \chi$
1^+	$\frac{4\pi}{3} (B_{10} ^2 \sin^2 \theta_A$ $+ B_{00} ^2 \cos^2 \theta_A)$	$\frac{4\pi}{3} (B_{10} ^2 \sin^2 \theta_\omega$ $+ B_{00} ^2 \cos^2 \theta_\omega)$	$\frac{4}{9} (4 B_{10} ^2 \cos^2 \chi$ $+ B_{00} ^2)$
2^-	$\frac{4\pi}{3} (3 B_{10} ^2 \sin^2 2\theta_A$ $+ B_{00} ^2 (3 \cos^2 \theta_A - 1)^2)$	$\frac{16\pi}{5} (B_{10} ^2 \sin^2 \theta_\omega$ $+ B_{00} ^2 \cos^2 \theta_\omega)$	$4 B_{10} ^2 \cos^2 \chi$ $+ B_{00} ^2$
2^+	$\pi B_{10} ^2 \sin^2 2\theta_A$	$\frac{4\pi}{5} B_{10} ^2 \sin^2 \theta_\omega$	$\frac{16}{15} B_{10} ^2 \sin^2 \chi$

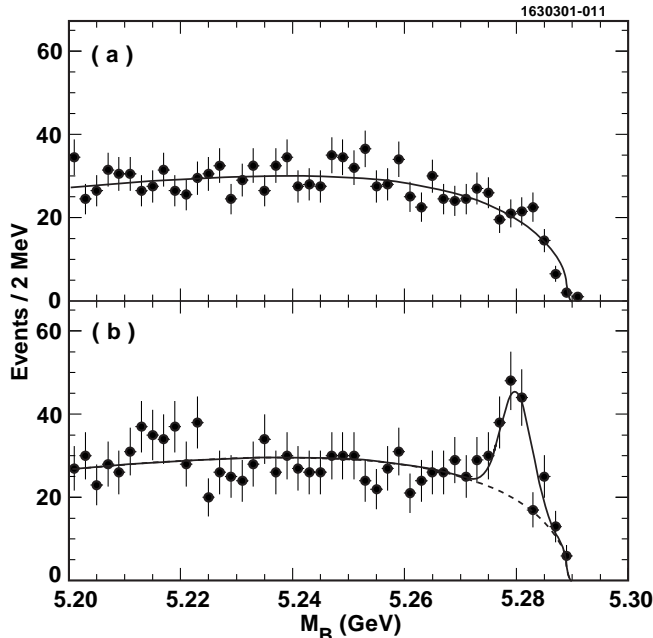


FIG. 17. The \bar{B} candidate mass spectra for the final state $D^0\omega\pi^-$, with $D^0 \rightarrow K^-\pi^+$. (a) for ΔE sidebands, and (b) for ΔE consistent with zero. The vertical scale in (a) was multiplied by 0.5 to facilitate comparison. The curve in (a) is a fit to the background distribution described in the text, while in (b) the shape from (a) is used with the normalization allowed to float and a signal Gaussian of width 2.7 MeV is added.

χ are fitted, integrating out the remaining degrees of freedom. Table V, gives the analytical form for these projections.

We determine the projections of these angular distributions by fitting the M_B distribution as a function of the various angular quantities $\cos\theta_A$, $\cos\theta_\omega$, χ . We restrict the $\omega\pi^-$ mass range to be between 1.1 and 1.7 GeV, containing 104 signal events. In order to fit the angular distribution with theoretical expectations, we must correct the data for acceptances. We determine the acceptance correction by comparing the Monte Carlo generated angular distributions with the reconstructed distributions. The angular dependent efficiencies are shown in Fig. 23.

The corrected angular distributions are shown in Fig. 24. The data are fit to the expectations for the various J^P assignments. For the 0^- , 1^- and 2^+ assignments, the curves have a fixed shape. For the 1^+ and 2^- assignments we let the ratio between the longitudinal and transverse amplitudes vary to best fit the data. We notice that the ω polarization is very clearly transverse ($\sin^2\theta_\omega$) and that infers a 1^- or 2^+ assignment.

We list in Table VI the χ^2/dof for the different J^P assignments. The 1^- assignment is preferred, having a χ^2/dof of 1.7. The other assignments are clearly ruled out. If the 1^- assignment is correct, the probability that our fit yields a χ^2/dof equal to 1.7 or greater is 3.8% [12].

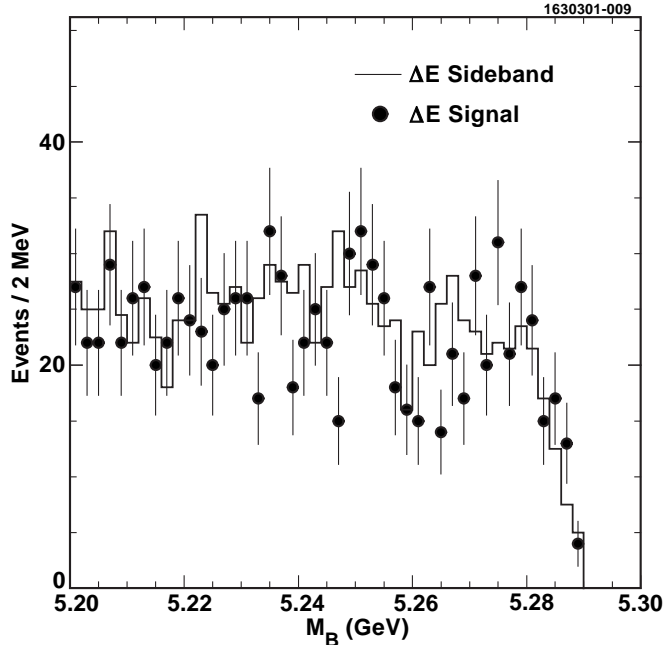


FIG. 18. The \bar{B} candidate mass spectra for the final state $D^0\omega\pi^-$, with $D^0 \rightarrow K^-\pi^+$ and ω sidebands for ΔE sidebands (histogram) and ΔE consistent with zero (points). The ΔE sideband numbers have been divided by 2.

TABLE VI. Results of fits to angular distributions

	0^-	1^+	1^-	2^+	2^-
χ^2/dof	7.0	4.5	1.7	3.2	5.3
dof	15	14	15	15	14
probability	1.9×10^{-15}	3.3×10^{-8}	3.8%	2.7×10^{-5}	3.3×10^{-10}

VIII. DISCUSSION OF NATURE OF THE A^-

We have found a 1^- object decaying into $\omega\pi^-$. A non-relativistic Breit-Wigner fit assuming a single resonance and no background gives a mass around 1420 MeV with an intrinsic width about 400 MeV. Signals for $\omega\pi^-$ resonances have been detected before below 1500 MeV. There is a well established axial-vector state, the $b_1(1235)$, with mass 1230 MeV and width 142 MeV. Data on vector states, excited ρ 's, are inconsistent. Clegg and Donnachie [13] have reviewed $\tau^- \rightarrow (4\pi)^-\bar{\nu}$, $e^+e^- \rightarrow \pi^+\pi^-$ and $e^+e^- \rightarrow \pi^+\pi^+\pi^-\pi^-$ data, including the $\omega\pi$ final state. Their best explanation is that of two 1^- states at 1463 ± 25 MeV and 1730 ± 30 MeV with widths 311 ± 62 and 400 ± 100 MeV, respectively. Only the lighter one decays into $\omega\pi$. The situation is quite complex, however. They conclude that these states must be mixed with non- $q\bar{q}$ states in order to explain their decay widths. There is also an observation of a wide, 300 MeV, $\omega\pi^0$ state in photoproduction at 1250 MeV [14], that is dominantly the $b_1(1235)$ [15] with possibly some 1^- in addition. Our state is consistent with the lower mass ρ' . We do not seem to be seeing significant production of the higher mass

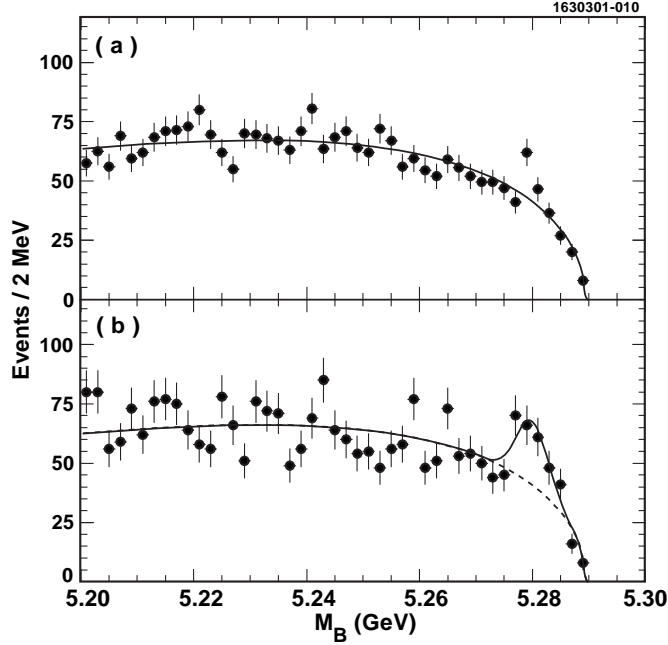


FIG. 19. The \overline{B} candidate mass spectra for the final state $D^+\omega\pi^-$, with $D^+ \rightarrow K^-\pi^+\pi^+$ (a) for ΔE sidebands and (b) for ΔE consistent with zero. The vertical scale in (a) was multiplied by 0.5 to facilitate comparison. The curve in (a) is a fit to the background distribution described in the text, while in (b) the shape from (a) is used with the normalization allowed to float and a signal Gaussian of width 2.7 MeV is added.

state into $\omega\pi^-$, as expected.

Several models predict the mass and decay widths of excited ρ and ω mesons. For example, according to Godfrey and Isgur [16] the first radial excitation of the ρ is at 1450 MeV. There is a large variation among the models, however, on prediction of the relative decay widths ranging from no $\pi\pi$ to $\pi\pi$ being equal to $\omega\pi$ [17].

Since we have observed a wide 1^- state in the mass region where the ρ' is expected, the most natural explanation is that we are observing the ρ' for the first time in B decays.

We note that τ^- lepton decays into $\omega\pi^-$ have been observed, and the 1^- spin-parity definitely established. However, the relatively low mass of the τ^- distorts the mass spectrum significantly, and makes it difficult to extract the ρ' mass and width [18] [19].

IX. MASS AND WIDTH VALUES FOR THE ρ'

Here we find the best values for the ρ' mass and width. This procedure is discussed in more detail in the Appendix. The shape of the $\omega\pi^-$ mass spectrum is affected by the phase space allowed by the B decay, the B decay amplitude, the decay amplitude for the ρ' , and finally the shape of the Breit-Wigner decay distribution. For $B \rightarrow D^{(*)}\omega\pi^-$ decay:

$$d\Gamma(B \rightarrow D^{(*)}\omega\pi) = \frac{1}{2M_B} |A(B \rightarrow D^{(*)}\rho') BW(\rho') A(\rho' \rightarrow \omega\pi)|^2 \times d\mathcal{P}(B \rightarrow D^{(*)}\rho') d\mathcal{P}(\rho' \rightarrow \omega\pi) \frac{dM_{\omega\pi}^2}{2\pi}, \quad (18)$$

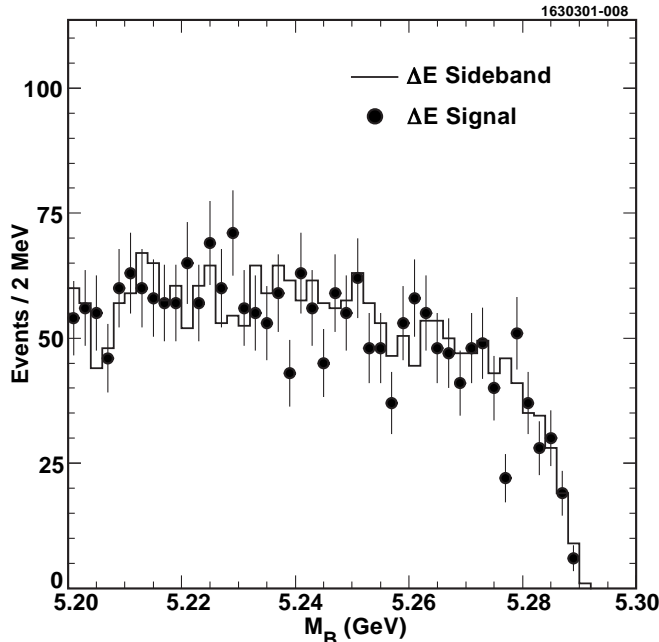


FIG. 20. The \bar{B} candidate mass spectra for the final state $D^+\omega\pi^-$, with $D^+ \rightarrow K^-\pi^+\pi^+$ and ω sidebands for ΔE sidebands (histogram) and ΔE consistent with zero (points). The ΔE sideband numbers have been divided by 2.

where $D^{(*)}$ indicates either a D^* or a D meson.

The phase space for two-body decays is well known. The decay amplitude for the B decay can be obtained from factorization where the ρ' is assumed to be identical to the lepton current [5]. Finally the Lorentz structure of the ρ' decay can be accounted for and we are left only to consider a Breit-Wigner amplitude of the form

$$\text{Breit - Wigner}(M_{\omega\pi}) = \frac{\Gamma(M_{\omega\pi})M_{\omega\pi}^2}{(M_{\omega\pi}^2 - M_{\rho'}^2)^2 + M_{\omega\pi}^2\Gamma^2(M_{\omega\pi})} , \quad (19)$$

where the mass dependent width is given by

$$\Gamma(M_{\omega\pi}) = \Gamma(M_{\rho'}) \left(\frac{p_{\omega}(M_{\omega\pi})}{p_{\omega}(M_{\rho'})} \right)^3 \left(\frac{M_{\rho'}}{M_{\omega\pi}} \right)^n \frac{1 + (Rp_{\omega}(M_{\rho'}))^2}{1 + (Rp_{\omega}(M_{\omega\pi}))^2} . \quad (20)$$

We allow the parameters R and n to float in the fit. They represent parameterizations of the hadronic matrix element and Blatt-Weiskopf damping factors. R is the ρ' radius in units of $\text{fm}/\hbar c$. Fig. 25 shows the fit to $M_{\omega\pi}$ distribution, where we have summed the D^0 , D^+ and D^{*+} data. (We have corrected the data in each channel for the $M_{\omega\pi}$ efficiency dependence, which is small for the D^0 and D^+ modes.)

The fit gives the mass and width to be $(1349 \pm 25_{-5}^{+10})$ MeV and $(547 \pm 86_{-45}^{+46})$ MeV, respectively. The errors are statistical and systematic; they are derived in the Appendix. The values for R and n are $2.05_{-1.14}^{+7.85}$ $\text{fm}/\hbar c$ and $0.57_{-0.83}^{+0.71}$, respectively.

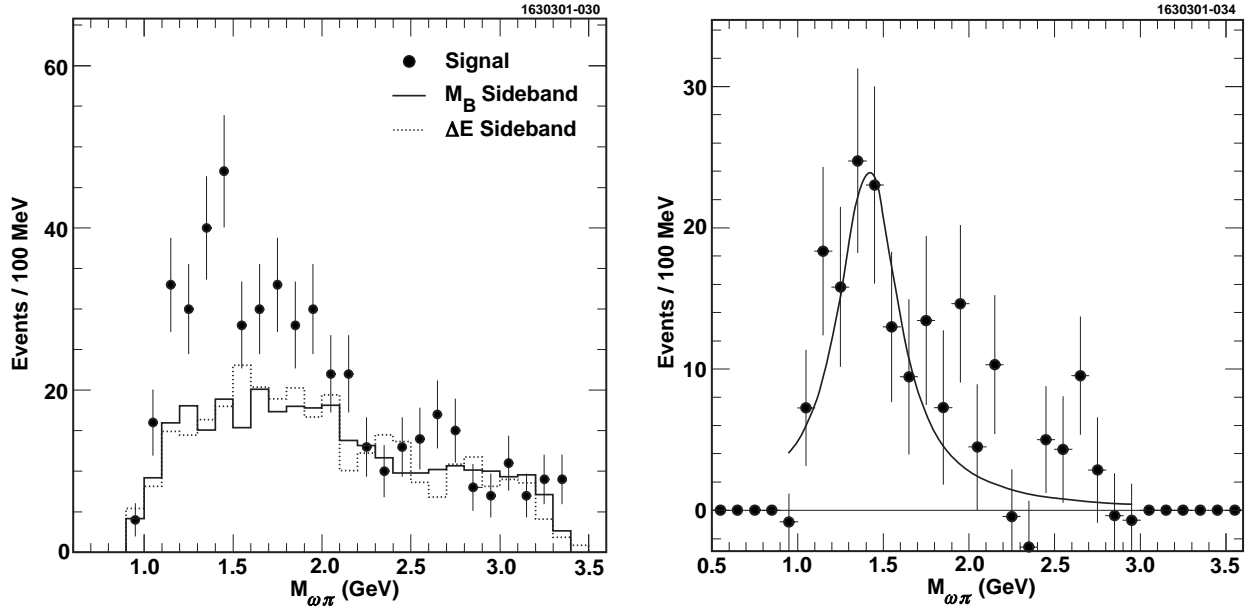


FIG. 21. The invariant mass spectra of $\omega\pi^-$ for the final state $D\omega\pi^-$ for both D decay modes. (left) The solid histogram is the background estimate from the M_B lower sideband and the dashed histogram is from the ΔE sidebands; both are normalized to the fitted number of background events. (right) The mass spectrum determined from fitting the M_B distribution and fit to a Breit-Wigner function. We find a peak value of 1415 ± 43 MeV and a width of 419 ± 110 MeV.

X. SEARCH FOR OTHER RESONANT SUBSTRUCTURE IN $D^*(4\pi)^-$

We have accounted for $\sim 20\%$ of the $(4\pi)^-$ final state. We would like to disentangle other resonant substructure. Since the background is large in modes other than $D^0 \rightarrow K^-\pi^+$ we will only use this mode. One process that comes to mind is that where the virtual W^- materializes as an a_1^- , that subsequently decays into $\pi^+\pi^-\pi^-$ and we produce a D^{*++} that decays into $D^{*+}\pi^0$. This process should be similar to that previously seen in the reaction $B^- \rightarrow D^{*0}\pi^-$, where the D^{*0} decayed into a $D^{*+}\pi^-$ [20]. We search for the presence of an a_1^- by examining the $\pi^+\pi^-\pi^-$ mass spectrum in Fig. 26.

There is an excess of signal events above background in the a_1^- mass region, that cannot be definitely associated with the a_1 . Proceeding by selecting events with $\pi^+\pi^-\pi^-$ masses between 0.6 and 1.6 GeV, we show the $D^{*+}\pi^0$ invariant mass spectrum in Fig. 27.

Although there is a suggestion of a low mass enhancement, it is not consistent with D^{**} production that would peak in region of 2.42 - 2.46 GeV. Perhaps we are seeing an indication of fragmentation at the $b \rightarrow c$ decay vertex here.

We also display for completeness the “ $a_1^-\pi^0$ ” mass distribution in Fig. 28. There may or may not be a wide structure in the $(4\pi)^-$ mass. At this point we abandon our search for substructure in this decay channel.

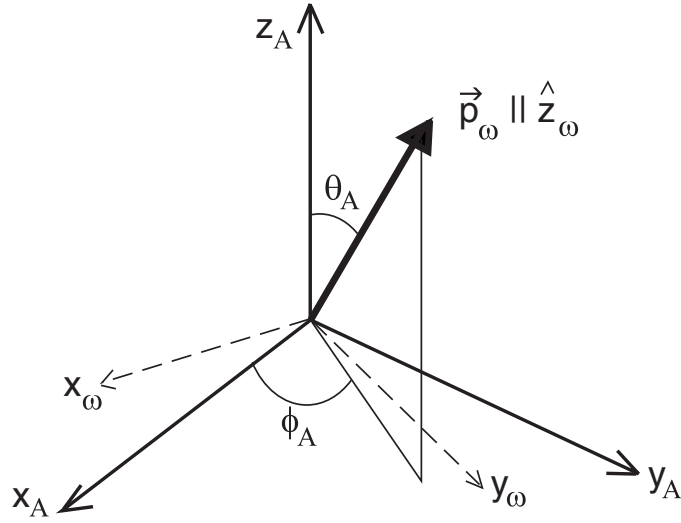


FIG. 22. Relationship between the A rest frame $x_A y_A z_A$ and the ω rest frame $x_\omega y_\omega z_\omega$. x_A and x_ω lie in the same plane.

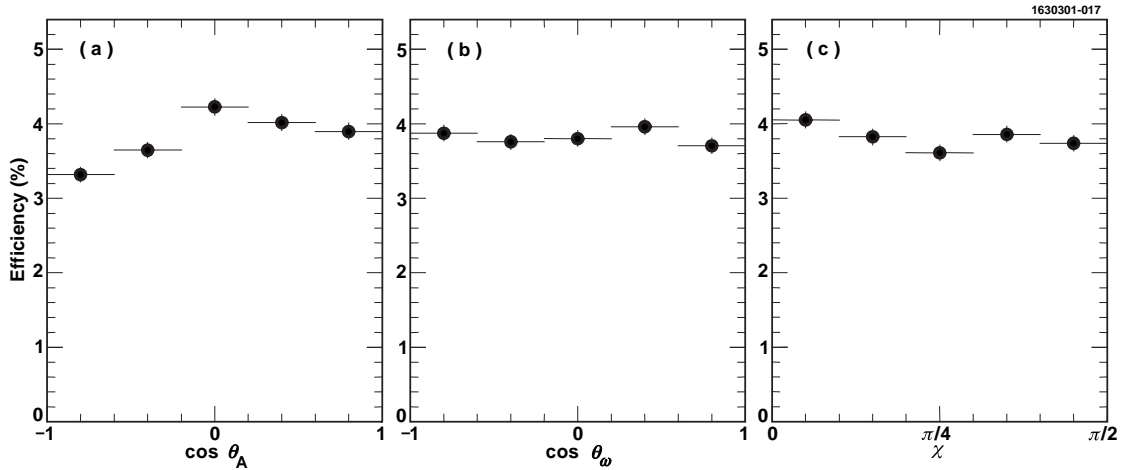


FIG. 23. Reconstruction efficiency dependence on (a) $\cos \theta_A$, (b) $\cos \theta_\omega$, and (c) χ .

XI. DISCUSSION AND CONCLUSIONS

We have made the first statistically significant observations of six hadronic B decays shown in Table VII.

There is a low-mass resonant substructure in the $\omega\pi^-$ mass. The fit to a sophisticated Breit-Wigner function gives the mass and width to be $(1349 \pm 25_{-5}^{+10})$ MeV and $(547 \pm 86_{-45}^{+46})$ MeV, respectively.

The structure at 1349 MeV has a spin-parity consistent with 1^- . It is likely to be the elusive ρ' resonance [13]. These are by far the most accurate and least model dependent measurements of the ρ' parameters. The ρ' dominates the final state. (Thus the branching ratios for the $D^{(*)}\omega\pi^-$ apply also for $D^{(*)}\rho'^-$.)

Heavy quark symmetry predicts equal partial widths for $D^*\rho'$ and $D\rho'$. We measure the

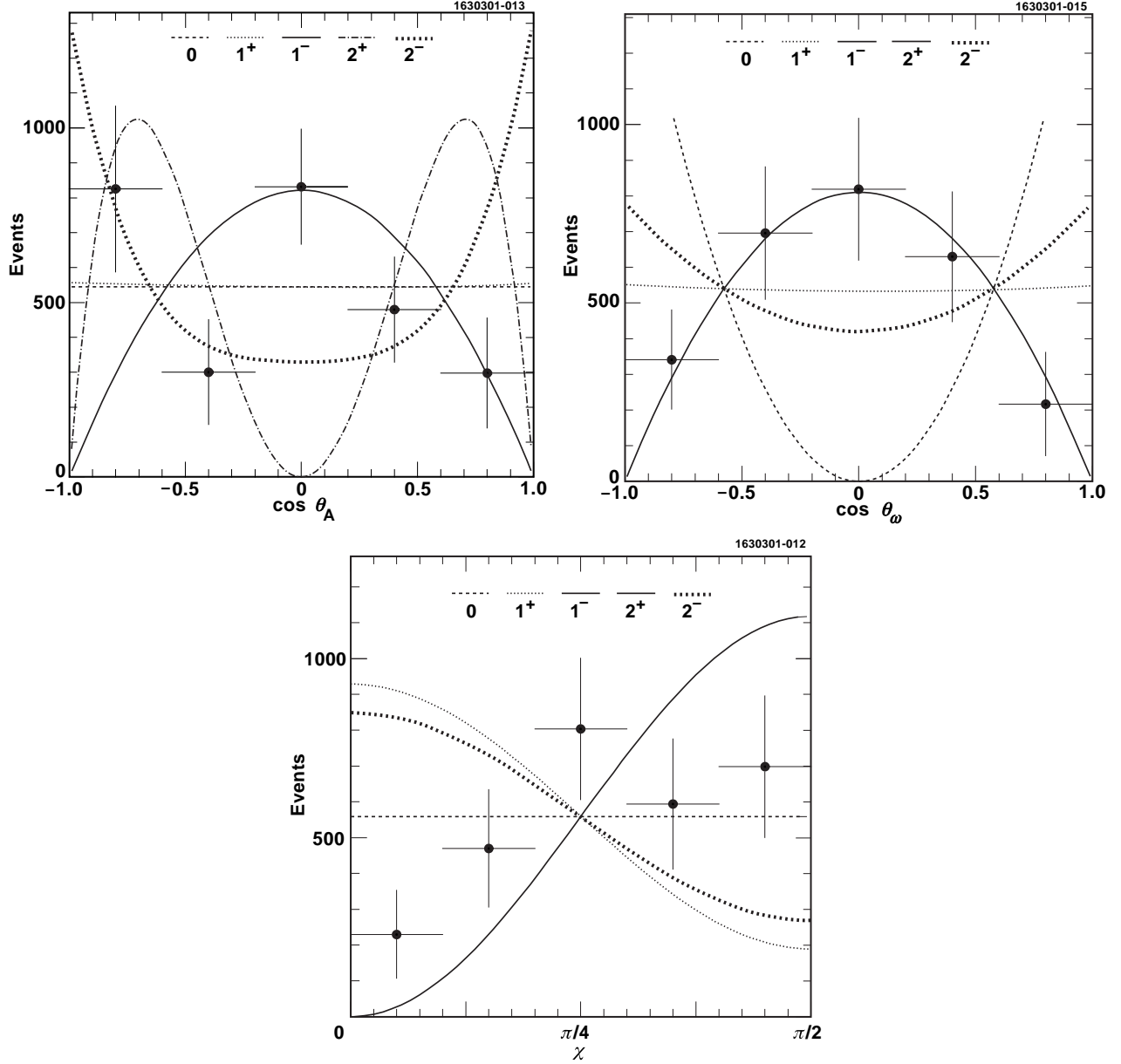


FIG. 24. The angular distribution of θ_A (top-left), θ_ω (top-right) and χ (bottom). The curves show the best fits to the data for different J^P assignments. (The 0^- and 1^+ are almost indistinguishable in $\cos \theta_A$, while the 1^- and 2^+ are indistinguishable in $\cos \theta_\omega$ and χ .)

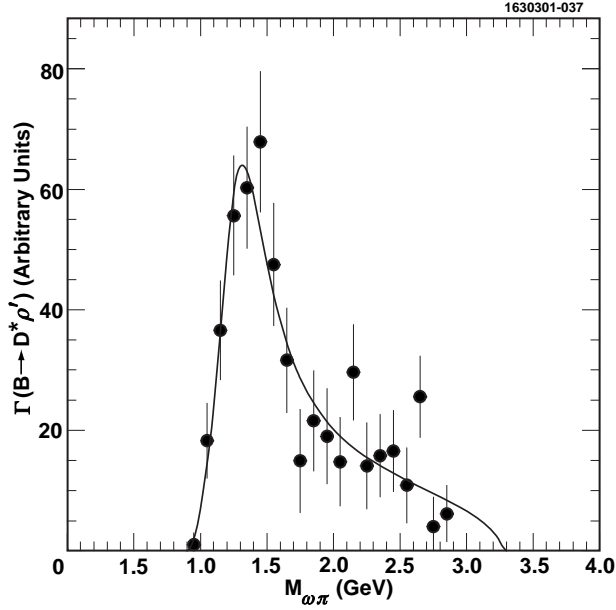


FIG. 25. Fit to the $M_{\omega\pi}$ distribution. The data in the D^0 , D^+ and D^{*+} channels have been summed and corrected using mass dependent efficiencies.

TABLE VII. Measured Branching Ratios

Mode	\mathcal{B} (%)	# of events
$\overline{B}^0 \rightarrow D^{*+}\pi^+\pi^-\pi^-\pi^0$	$1.72 \pm 0.14 \pm 0.24$	1230 ± 70
$\overline{B}^0 \rightarrow D^{*+}\omega\pi^-$	$0.29 \pm 0.03 \pm 0.04$	136 ± 15
$\overline{B}^0 \rightarrow D^+\omega\pi^-$	$0.28 \pm 0.05 \pm 0.04$	91 ± 18
$B^- \rightarrow D^{*0}\pi^+\pi^-\pi^-\pi^0$	$1.80 \pm 0.24 \pm 0.27$	195 ± 26
$B^- \rightarrow D^{*0}\omega\pi^-$	$0.45 \pm 0.10 \pm 0.07$	26 ± 6
$B^- \rightarrow D^0\omega\pi^-$	$0.41 \pm 0.07 \pm 0.06$	88 ± 14

relative rates to be

$$\frac{\Gamma(\overline{B}^0 \rightarrow D^{*+}\rho'^-)}{\Gamma(\overline{B}^0 \rightarrow D^+\rho'^-)} = 1.04 \pm 0.21 \pm 0.06 \quad (21)$$

$$\frac{\Gamma(B^- \rightarrow D^{*0}\rho'^-)}{\Gamma(B^- \rightarrow D^0\rho'^-)} = 1.10 \pm 0.31 \pm 0.06 \quad (22)$$

$$\frac{\Gamma(\overline{B} \rightarrow D^*\rho'^-)}{\Gamma(\overline{B} \rightarrow D\rho'^-)} = 1.06 \pm 0.17 \pm 0.04 \quad . \quad (23)$$

Thus the prediction of heavy quark symmetry is satisfied within our errors.

Factorization predicts that the fraction of longitudinal polarization of the D^{*+} is the same as in the related semileptonic decay $\overline{B} \rightarrow D^*\ell^-\bar{\nu}$ at four-momentum transfer q^2 equal to the mass-squared of the ρ' [5]

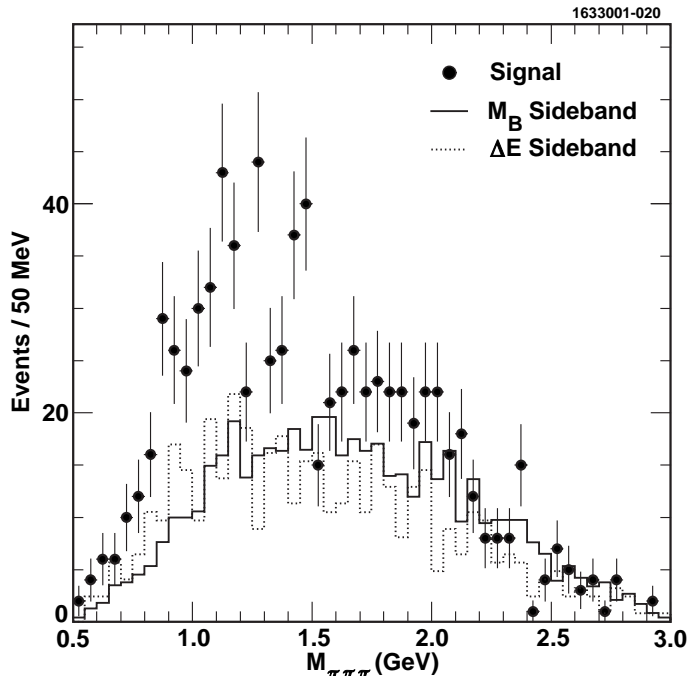


FIG. 26. The invariant mass spectra of $\pi^+\pi^-\pi^-$ for the final state $D^{*+}\pi^+\pi^-\pi^0$ for $D^0 \rightarrow K^-\pi^+$. The solid histogram is the background estimate from the M_B lower sideband and the dashed histogram is from the ΔE sidebands; both are normalized to the fitted number of background events.

$$\frac{\Gamma_L(\overline{B} \rightarrow D^{*+}\rho'^-)}{\Gamma(\overline{B} \rightarrow D^{*+}\rho'^-)} = \frac{\Gamma_L(\overline{B} \rightarrow D^*\ell^-\bar{\nu})}{\Gamma(\overline{B} \rightarrow D^*\ell^-\bar{\nu})} \Big|_{q^2=m_{\rho'}^2} \quad . \quad (24)$$

Our measurement of the D^{*+} polarization (see Fig. 15) is $(63 \pm 9)\%$. The model predictions in semileptonic decays for a q^2 of 2 GeV^2 , are between 66.9 and 72.6% [21]. Thus this prediction of factorization is satisfied.

We can use factorization to estimate the product of the ρ' weak decay constant $f_{\rho'}$ and the branching ratio for $\rho'^- \rightarrow \omega\pi^-$. The relevant expression is

$$\frac{\Gamma(\overline{B} \rightarrow D^{*+}\rho'^-, \rho'^- \rightarrow \omega\pi^-)}{\frac{d\Gamma}{dq^2}(\overline{B} \rightarrow D^*\ell^-\bar{\nu})|_{q^2=m_{\rho'}^2}} = 6\pi^2 c_1^2 f_{\rho'}^2 \mathcal{B}(\rho'^- \rightarrow \omega\pi^-) |V_{ud}|^2 \quad , \quad (25)$$

where c_1 is a QCD correction factor. We use $c_1 = 1.1 \pm 0.1$ [22].

We use the semileptonic decay rates given in Barish *et al.* [23]. The product

$$f_{\rho'}^2 \mathcal{B}(\rho'^- \rightarrow \omega\pi^-) = 0.011 \pm 0.003 \text{ GeV}^2 \quad , \quad (26)$$

where the error is the quadrature of the experimental errors on the experimental branching ratios and c_1 .

The model of Godfrey and Isgur predicts decay constants widths and partial widths of mesons comprised of light quarks by using a relativistic treatment in the context of QCD

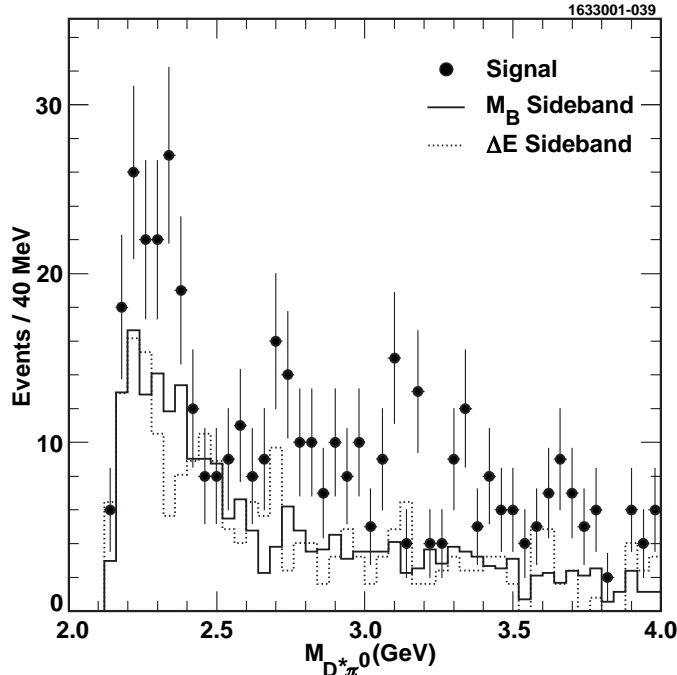


FIG. 27. The invariant mass spectra of $D^{*+}\pi^0$ for $\pi^+\pi^-\pi^-$ masses between 0.6 - 1.6 GeV for the final state $D^{*+}\pi^+\pi^-\pi^-\pi^0$ with $D^0 \rightarrow K^-\pi^+$. The solid histogram is the background estimate from the M_B lower sideband and the dashed histogram is from the ΔE sidebands; both are normalized to the fitted number of background events.

[16]. They predict both $f_{\rho'}$ and $\mathcal{B}(\rho'^- \rightarrow \omega\pi^-)$; the values are 80 MeV and 39%, respectively. The branching ratio prediction is believed to be more accurate [24]. We use this to extract

$$f_{\rho'} = 167 \pm 23 \text{ MeV} . \quad (27)$$

The model predicts a lower value for $f_{\rho'}$ than observed here, if factorization is correct.

We note that all the $B \rightarrow D^{(*)}\rho'$ branching ratios that we have measured are approximately equal to the $B \rightarrow D^{(*)}\rho$ branching rates [4] if a model value of $\mathcal{B}(\rho'^- \rightarrow \omega\pi^-) = 39\%$ is used.

Finally, although the $\overline{B}^0 \rightarrow D^{*+}(4\pi)^-$ and $B^- \rightarrow D^{*0}(4\pi)^-$ branching ratios are nearly equal, the $\omega\pi^-$ branching ratios are about 1.5 times larger for the charged B than the neutral B , maintaining the trend seen for the π^- and ρ^- final states. Since the B^- lifetime is if anything longer than the B^0 , this trend must reverse for some final states. It has not for $D^{(*)}\rho'$.

XII. ACKNOWLEDGEMENTS

We thank A. Donnachie, N. Isgur, J. Rosner and J. Schechter for useful discussions. We also thank D. Black of Syracuse University for crucial insights on how to calculate Lorentz structures. We gratefully acknowledge the effort of the CESR staff in providing us with excellent luminosity and running conditions. M. Selen thanks the PFF program of the NSF and the Research Corporation, and A.H. Mahmood thanks the Texas Advanced Research Pro-

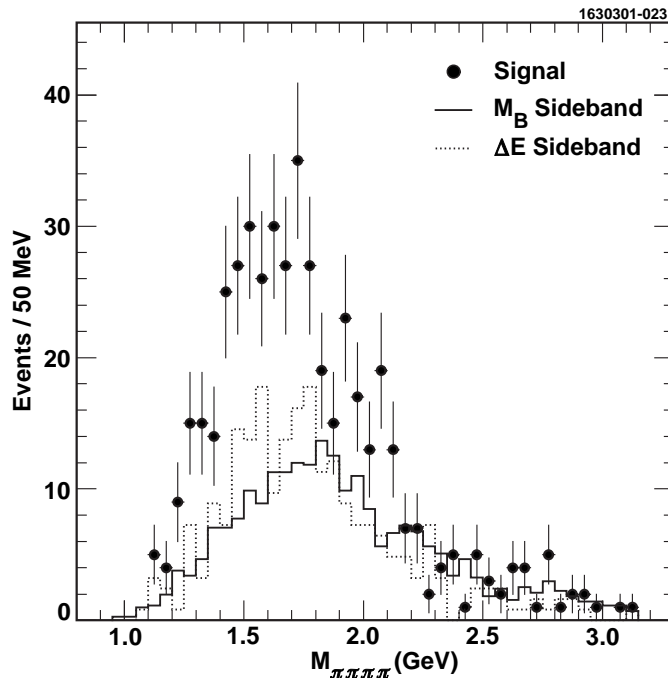


FIG. 28. The invariant mass spectra of $\pi^+\pi^-\pi^-\pi^0$ for $\pi^+\pi^-\pi^-$ masses between 0.6 - 1.6 GeV for the final state $D^{*+}\pi^+\pi^-\pi^0$ with $D^0 \rightarrow K^-\pi^+$. The solid histogram is the background estimate from the M_B lower sideband and the dashed histogram is from the ΔE sidebands; both are normalized to the fitted number of background events.

gram. This work was supported by the National Science Foundation, the U.S. Department of Energy, and the Natural Sciences and Engineering Research Council of Canada.

REFERENCES

- [1] D. Groom *et al.*, The Eur. Phys. Journ. C **15**, 1 (2000).
- [2] CLEO Collaboration, G. Brandenburg *et al.*, Phys. Rev. D **61**, 072002 (2000).
- [3] ARGUS previously reported a signal of 28 ± 10 events in this mode, corresponding to a branching ratio of $(3.4 \pm 1.8)\%$. H. Albrecht *et al.*, Z. Phys. C **48**, 543 (1990).
- [4] CLEO Collaboration, M. Alam *et al.*, Phys. Rev. D **50**, 43 (1994); CLEO Collaboration, B. Barish *et al.*, “Exclusive Reconstruction of $B \rightarrow D^{(*)}(n\pi)^-$ Decays,” CONF 97-01, EPS 339 (1997).
- [5] J. Bjorken, Nucl. Phys. B (Proc. Suppl.) **11**, 325 (1989); D. Bortoletto and S. Stone, Phys. Rev. Lett. **65**, 2951 (1990); M. J. Dugan and B. Grinstein Phys. Lett. **B255**, 583 (1991) and references contained therein; T. E. Browder, K. Honscheid and S. Playfer, in *B Decays* Revised 2nd Ed., ed. S. Stone (World Scientific, Singapore (1994), p158 and references contained therein.
- [6] The CLEO II detector is described in Y. Kubota *et al.*, Nucl. Instrum. Methods A **320**, 66 (1992), and CLEO II.V in T. Hill, *ibid* A **418**, 32 (1998).
- [7] G. Fox and S. Wolfram, Phys. Rev. Lett. **23**, 1581 (1978).
- [8] We do not find significant differences between the CLEO II and II.V data sets.
- [9] D. H. Perkins, *Introduction to High Energy Physics* 2nd Ed., (Addison-Wesley, Reading, 1982), p. 136, 1982; B. C. Maglic *et al.*, Phys. Rev. Lett. **7**, 178 (1961).
- [10] We assume that $\omega\pi$ is in a 1^- final state. The difference between the efficiency of a 1^- system and an uncorrelated decay distribution is less than 2%.
- [11] M. Jacob and G.C. Wick, *Ann. Phys. (N.Y.)* **7** (1959) 404; J. D. Jackson, in *High Energy Physics, Les Houches, 1965*, (Gordon and Breach, NY, 1966); M.L. Perl, *High Energy Hadron Physics*, (Wiley, NY, 1974).
- [12] We allowed a systematic error of 5.5% on the number of events in each angular bin resulting possibly from the fitting procedure to the M_B spectrum. This changed the probability of χ^2 for the 1^- case to 3.9% from 3.8%, and caused negligible changes in the other cases.
- [13] A. B. Clegg and A. Donnachie, Z. Phys. **C 62**, 455 (1994).
- [14] D. Aston *et al.*, Nucl. Phys. **B234**, 1 (1984).
- [15] J. Brau *et al.*, Phys. Rev. D **37**, 2379 (1988).
- [16] S. Godfrey and N. Isgur, Phys. Rev. D **32**, 189 (1985).
- [17] G. Busetto and N. Oliver, Z. Phys. **C 20**, 247 (1983); R. Kokoski and N. Isgur, Phys. Rev. D **35**, 907 (1987).
- [18] CLEO Collaboration, K. Edwards *et al.* (CLEO), Phys. Rev. D **61**, 072003 (2000).
- [19] The ρ' mass and width are also estimated from $\tau^- \rightarrow \pi^+\pi^0\nu_\tau$ decays, but the large interference from the $\rho(770)$ tail causes these results to have large uncertainties. See CLEO Collaboration, S. Anderson *et al.*, Phys. Rev. D **61**, 112002 (2000).
- [20] CLEO Collaboration, M. S. Alam *et al.*, Phys. Rev. D **50**, 43 (1994); CLEO Collaboration, S. Anderson *et al.*, “Observation of a Broad $L = 1$ cq state in $B^- \rightarrow D^{*+}\pi^-\pi^-$ at CLEO,” CONF 99-6 (1999).
- [21] N. Isgur and M. B. Wise, Phys. Lett. **B237**, 527 (1990); M. Wirbel *et al.*, Z. Phys. **C29**, 627 (1985); N. Neubert, Phys. Lett. **B264**, 455 (1991).
- [22] The error is due to the uncertainty in the scale where the Wilson coefficients are eval-

- uated. See T. Browder, K. Honscheid and S. Playfer, in *B Decays* 2nd Ed., ed. by S. Stone, (World Scientific, Singapore, 1994).
- [23] CLEO Collaboration, B. Barish *et al.*, Phys. Rev. D **51**, 1014 (1995). We correct for the new value of the $D^0 \rightarrow K^- \pi^+$ branching ratio.
- [24] Private communication from N. Isgur. The decay constants given in ref. [16] are dimensionless and must be multiplied by m to put them in the convention used here. An additional factor of $\sqrt{2}$ must be used to convert from the electromagnetic form-factor to the weak form-factor using CVC.
- [25] S. Stone, *B Decays* Revised 2nd Ed., (World Scientific, Singapore, 1994).
- [26] M. Neubert, Phys. Reports **245** (1994), 259.
- [27] F. E. Close and A. Wambach, Nucl. Phys. **B412** 169 (1994).
- [28] J. E. Duboscq *et al.*, Phys. Rev. Lett. **76** 3898 (1996).
- [29] J. Blatt and V. F. Weisskopf, *Theoretical Nuclear Physics*, (John Wiley and Sons, NY, 1952).
- [30] F. Halzen and A. D. Martin, *Quarks and Leptons*, (John Wiley and Sons, NY, 1984).

XIII. APPENDIX: DETERMINATION OF THE ρ' MASS AND WIDTH

A. Introduction

Since the ρ' decays to $\omega\pi^-$ via a P-wave, we need to take into account the fact that the width, $\Gamma(M_{\omega\pi})$, may not be constant, but can vary with $M_{\omega\pi}$. Furthermore we need to consider the kinematic limits from $B \rightarrow D^{(*)}\rho'$ decay and $\rho' \rightarrow \omega\pi$ decay.

B. The Differential Decay Distribution

We can write a general expression for the differential distribution for $M_{\omega\pi}$ in $d\Gamma(B \rightarrow D^{(*)}\omega\pi)$ via the ρ' as:

$$d\Gamma(B \rightarrow D^{(*)}\omega\pi) = \frac{1}{2M_B} |A(B \rightarrow D^{(*)}\rho') BW(\rho') A(\rho' \rightarrow \omega\pi)|^2 \quad (28)$$

$$\times d\mathcal{P}(B \rightarrow D^{(*)}\rho') d\mathcal{P}(\rho' \rightarrow \omega\pi) \frac{dM_{\omega\pi}^2}{2\pi},$$

where $d\mathcal{P}$ indicates a phase space term, BW indicates some form of a Breit-Wigner shape function, and A indicates an amplitude.

The phase space of $B \rightarrow D^{(*)}\rho'$ provides a cut off at higher $M_{\omega\pi}$, whereas the phase space of $\rho' \rightarrow \omega\pi$ provides a cut off at lower $M_{\omega\pi}$. We assume that the two decay stages are independent and can be factorized. Thus the function can be calculated from the widths of B and ρ' decays.

1. The B Decay Width

The width for ρ' production is given by:

$$\Gamma(B \rightarrow D^{(*)} \rho') = \frac{1}{2M_B} |A(B \rightarrow D^{(*)} \rho')|^2 d\mathcal{P}(B \rightarrow D^* \rho') \quad (29)$$

$$d\mathcal{P}(B \rightarrow D^{(*)} \rho') = \frac{1}{8\pi} \left(\frac{2p_{D^*}}{M_B} \right) \quad (30)$$

$$A(B \rightarrow D^{(*)} \rho') \sim \sqrt{G_F} V_{cb} \times \text{Lorentz structure} \times f_{\rho'}(M_{\omega\pi})$$

where $f_{\rho'}(M_{\omega\pi})$ is the ρ' weak production form factor.

Instead of having to calculate $f_{\rho'}(M_{\omega\pi})$, we can use our knowledge of semileptonic b decays, $B \rightarrow D^{(*)} \ell^- \bar{\nu}$ coupled with factorization to approximate $A(B \rightarrow D^* \rho')$.

Factorization tells us:

$$\begin{aligned} \Gamma(B \rightarrow D^{(*)} \rho') &= 6\pi^2 |V_{ud}|^2 f_{\rho'}^2(M_{\omega\pi}) |a_1|^2 \frac{d\Gamma(B \rightarrow D^{(*)} l\nu)}{dq^2} \Big|_{q^2=M_{\omega\pi}^2} \quad (31) \\ &\propto p_{D^{(*)}} M_{\omega\pi}^2 \times \{|H_+(M_{\omega\pi}^2)|^2 + |H_-(M_{\omega\pi}^2)|^2 + |H_o(M_{\omega\pi}^2)|^2\} \end{aligned}$$

The helicity amplitudes $H(M_{\omega\pi}^2)$ can be related to the axial-vector form factors $A_1(q^2)$ and $A_2(q^2)$, and vector form factor $V(q^2)$. Details can be found in reference [25].

$$H_{\pm}(q^2) = (M_B + M_{D^*}) A_1(q^2) \mp \frac{2M_B p_{D^*}}{M_B + M_{D^*}} V(q^2) \quad (32)$$

$$H_o(q^2) = \frac{1}{2M_{D^*} \sqrt{q^2}} \left[(M_B^2 - M_{D^*}^2 - q^2)(M_B + M_{D^*}) A_1(q^2) - \frac{4M_B^2 p_{D^*}^2}{M_B + M_{D^*}} A_2(q^2) \right]$$

In the heavy-quark symmetry limit, the form factors A_1, A_2 , and V are related to the Isgur-Wise function. With correction due to finite heavy quark mass and α_s , they can be written as

$$\begin{aligned} A_1(q^2) &= \left[1 - \frac{q^2}{(M_B + M_{D^*})^2} \right] \frac{M_B + M_{D^*}}{2\sqrt{M_B M_{D^*}}} h_{A_1}(w) \quad (33) \\ A_2(q^2) &= R_2 \frac{M_B + M_{D^*}}{2\sqrt{M_B M_{D^*}}} h_{A_1}(w) \\ V(q^2) &= R_1 \frac{M_B + M_{D^*}}{2\sqrt{M_B M_{D^*}}} h_{A_1}(w) \quad , \end{aligned}$$

where w is the invariant four-velocity transfer.

The values calculated by Neubert for R_1 and R_2 have the explicit dependence on w [26] of

$$\begin{aligned} R_1(w) &= 1.35 - 0.22(w - 1) + 0.09(w - 1)^2 \quad (34) \\ R_2(w) &= 0.79 + 0.15(w - 1) - 0.04(w - 1)^2 \quad , \end{aligned}$$

while Close and Wambach [27] determine

$$\begin{aligned} R_1(w) &= 1.15 - 0.07(w - 1) + \mathcal{O}(w - 1)^2 \quad (35) \\ R_2(w) &= 0.91 + 0.04(w - 1) + \mathcal{O}(w - 1)^2 \quad . \end{aligned}$$

CLEO measured $R_1(0)$ and $R_2(0)$ to be $1.18 \pm 0.30 \pm 0.12$ and $0.71 \pm 0.22 \pm 0.07$, respectively [28]. The form factor $h_{A_1}(w)$ can be assumed to be linear as $h_{A_1}(w) = 1 - \rho_{A_1}^2(w - 1)$; CLEO measured $\rho_{A_1}^2$ to be $0.91 \pm 0.15 \pm 0.06$.

$\Gamma(B \rightarrow D^* \rho')$ as function of $M_{\omega\pi}$ is shown in Fig. 29, where the form factor $f_{\rho'}$ is not included.

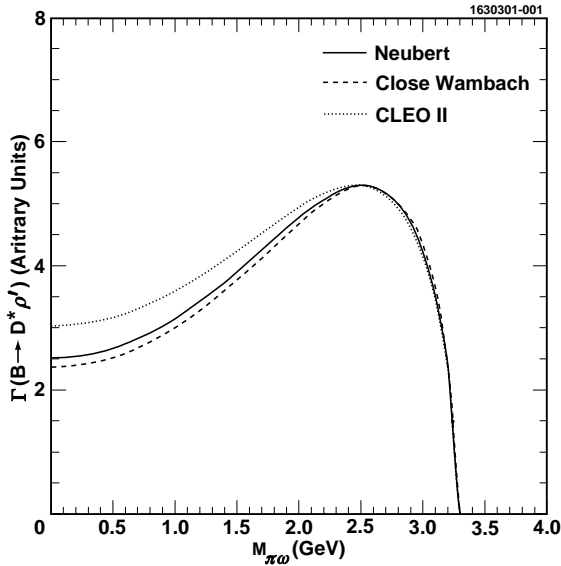


FIG. 29. Decay width of $B \rightarrow D^* \rho'$ as function of $M_{\omega\pi}$. The parameters R_1 and R_2 are from Neubert (solid line), Close and Wambach (dashed line) and the CLEO measurement (dotted line), with $\rho_{A_1}^2$ as 0.91.

2. The Width of ρ' decay

The width of ρ' decay can be expanded as:

$$\Gamma(\rho' \rightarrow \omega\pi) = \frac{1}{2M_{\omega\pi}} |A(\rho' \rightarrow \omega\pi)|^2 d\mathcal{P}(\rho' \rightarrow \omega\pi) \quad (36)$$

$$d\mathcal{P}(\rho' \rightarrow \omega\pi) = \frac{1}{8\pi} \left(\frac{2p_\omega}{M_{\omega\pi}} \right) \quad (37)$$

$$A(\rho' \rightarrow \omega\pi) = \text{Lorentz structure} \times h(M_{\omega\pi}^2) \quad , \quad (38)$$

where p_ω is evaluated in the $\omega\pi$ rest frame, and $h(M_{\omega\pi}^2)$ is the ρ' strong decay form factor, which is usually assumed to be a constant.

The Lorentz structure of $\rho' \rightarrow \omega\pi$ must be linear in the polarization vectors of the ρ' and the ω . The simplest mathematical expression is $\varepsilon_{\rho'} \cdot \varepsilon_\omega$, which is S-wave. For P-wave, since $\varepsilon_{\rho'} \cdot p_{\rho'} = 0$ and $\varepsilon_\omega \cdot p_\omega = 0$ by transversality, the only Lorentz scalars we can form are $(\varepsilon_{\rho'} \cdot p_\omega)(\varepsilon_\omega \cdot p_{\rho'})$ and $\epsilon_{\mu\nu\alpha\beta} \varepsilon_{\rho'}^\mu \varepsilon_\omega^\nu p_\omega^\alpha p_{\rho'}^\beta$. The first term violates parity conservation. Later, we describe the detailed calculation of the second term, which gives

$$|A(\rho' \rightarrow \omega\pi)|^2 = h^2(M_{\omega\pi}^2) |\epsilon_{\mu\nu\alpha\beta} \varepsilon_{\rho'}^\mu \varepsilon_\omega^\nu p_\omega^\alpha p_{\rho'}^\beta|^2 \propto h^2(M_{\omega\pi}^2) M_{\omega\pi}^2 p_\omega^2 \quad (39)$$

Thus, the width of $\rho' \rightarrow \omega\pi$ is:

$$\Gamma(\rho' \rightarrow \omega\pi) \propto h^2(M_{\omega\pi}^2) p_\omega^3 \quad (40)$$

Note, that the contribution of longitudinal polarized ω to the width is zero, which is consistent with our spin-parity study; our measurements gave $\Gamma_{Long}/\Gamma_{tot}$ to be $(10 \pm 9)\%$ in the $D^*\omega\pi$ mode and $(-0.4 \pm 22\%)$ in the $D\omega\pi$ mode.

3. The Breit-Wigner

The Breit-Wigner function has a long history. Fundamentally we are approximating the decay as having a non-changing amplitude as a function of mass in the simplest case. In general the denominator of the Breit-Wigner has a fixed form in amplitude given by

$$\text{Denominator} = M_{\omega\pi}^2 - M_{\rho'}^2 - iM_{\omega\pi}\Gamma_{tot}(M_{\omega\pi}) \quad , \quad (41)$$

The numerator is where we have to have more discussion. Since $\omega\pi$ is a large decay mode of ρ' , we assume that the mass dependence of Γ_{tot} can be approximated by the mass dependence of $\Gamma_{\omega\pi}$

$$\Gamma_{tot}(M_{\omega\pi}) = \Gamma_{tot}(M_{\rho'}) \frac{\Gamma_{\omega\pi}(M_{\omega\pi})}{\Gamma_{\omega\pi}(M_{\rho'})} \quad (42)$$

From the derivation of $\Gamma(\rho' \rightarrow \omega\pi)$ above, we see that

$$\frac{\Gamma_{\omega\pi}(M_{\omega\pi})}{\Gamma_{\omega\pi}(M_{\rho'})} = \left(\frac{h(M_{\omega\pi}^2)}{h(M_{\rho'}^2)} \right)^2 \times \left(\frac{p_{\omega}(M_{\omega\pi})}{p_{\omega}(M_{\rho'})} \right)^3 \quad (43)$$

4. The Differential Distribution

Eq. 29 now can be rewritten as:

$$d\Gamma(B \rightarrow D^*\omega\pi) = \Gamma(B \rightarrow D^*\rho') \frac{2M_{\omega\pi}\Gamma_{\omega\pi}(M_{\omega\pi})}{(M_{\omega\pi}^2 - M_{\rho'}^2)^2 + M_{\omega\pi}^2\Gamma_{tot}(M_{\omega\pi})^2} \frac{dM_{\omega\pi}^2}{2\pi} \quad (44)$$

With the relation shown in Eq. 42, we have the differential function which can be used for fitting the mass distribution:

$$\frac{d\Gamma(B \rightarrow D^*\omega\pi)}{dM_{\omega\pi}} = C \times \Gamma(B \rightarrow D^*\rho') \times \frac{\Gamma M_{\omega\pi}^2}{(M_{\omega\pi}^2 - M_{\rho'}^2)^2 + M_{\omega\pi}^2\Gamma^2} \quad , \quad (45)$$

where Γ is the $M_{\omega\pi}$ -dependent total width. From Eq. 42 and Eq. 43 we get that:

$$\Gamma = \Gamma_0 \times \left(\frac{h(M_{\omega\pi}^2)}{h(M_{\rho'}^2)} \right)^2 \times \left(\frac{p_{\omega}(M_{\omega\pi})}{p_{\omega}(M_{\rho'})} \right)^3 \quad (46)$$

5. Decay Form Factor of $\rho' \rightarrow \omega\pi$

Now, what form should we use for $h(M_{\omega\pi}^2)$? In Eq. 39, the dimensions of $h(M_{\omega\pi}^2)$ are GeV^{-1} . But the dependence on $M_{\omega\pi}$ could be anything. So we can try $h(M_{\omega\pi}^2) \propto M_{\omega\pi}^n$, where n is allowed to float in the fit.

$h(M_{\omega\pi}^2)$ could also include Blatt-Weisskopf factors [29]. A Blatt-Weisskopf factor for the P-wave decay $\rho' \rightarrow \omega\pi$ would be of the form:

$$FF(M_{\omega\pi}^2) = \frac{1 + (Rp_{\omega}(M_{\rho'}))^2}{1 + (Rp_{\omega}(M_{\omega\pi}))^2} \quad (47)$$

where R is the radius of the ρ' meson. A typical value is $R = 1 \text{ fm}/\hbar c$.

C. Fit to $M_{\omega\pi}$ Spectrum

Since we are limited by the statistics, we chose to add the D and D^* final states together. This is permissible since the Lorentz structure of ρ' decay in the different modes is the same. The only difference is in the width of $B \rightarrow D^{(*)}\rho'$ part, that depends on $M_{\omega\pi}$, however this difference is slight.

We use following formula to represent the width:

$$\Gamma(M_{\omega\pi}) = \Gamma(M_{\rho'}) \left(\frac{p_{\omega}(M_{\omega\pi})}{p_{\omega}(M_{\rho'})} \right)^3 \left(\frac{M_{\rho'}}{M_{\omega\pi}} \right)^n \frac{1 + (Rp_{\omega}(M_{\rho'}))^2}{1 + (Rp_{\omega}(M_{\omega\pi}))^2} \quad (48)$$

We allow the parameters R and n to float. We use Neubert's calculated values for R_1 and R_2 ; effects of changing this to other estimates will contribute to the systematic error. Fig. 25 shows the fit to $M_{\omega\pi}$ distribution.

The fit gives the mass and width to be (1349 ± 25) MeV and (547 ± 86) MeV, respectively. The values for R and n are $2.05^{+7.85}_{-1.14}$ and $0.57^{+0.71}_{-0.83}$, respectively.

Systematic errors can arise from several sources. We test our fit globally by restricting the mass range to below 1.8 GeV. This results in a shift in the mass by -5.7 MeV and the width by -23.2 MeV. Both of these changes are much smaller than the statistical error.

Two specific sources of systematic error are using the D^* mass to represent both D^* and D meson final states, and using the form-factors R_1 and R_2 from Neubert's calculation. To estimate the error on the former, we use the D in the fit; for the latter we use form-factors as calculated by Close and Wambach or, the CLEO measurement of these parameters. Listed in the Table VIII are the contributions from each of these sources.

Finally, to estimate the error due to our model of the $\omega\pi^-$ shape, we allow the values of R and n to change so that the χ^2 of the fit increases by one unit, corresponding to a one standard deviation variation. We list in Table VIII the maximum positive and negative changes in the mass and width values allowed by these variations. Thus our final value for the mass of ρ' resonance is $(1349 \pm 25^{+10}_{-5})$ MeV. The width is $(547 \pm 86^{+46}_{-45})$ MeV.

TABLE VIII. Mass and width fit of resonance ρ'

Parameters	Mass (MeV)	Width (MeV)
Neubert (nominal)	1349 ± 25	547 ± 86
$M = M_D$	-4.0	-31
Close-Wambach	-1.5	-9
CLEO $D^*l\nu$	+8.2	+24
Vary R and n	+5.8 -3.2	+40 -31
Systematic error	+10.0 -5.3	+46 -45

It is possible that values of the ρ' mass and width could be affected if additional resonance substructure of unknown origin were to be included. There is no evidence, however, that such structures are needed. By including all the known physics effects of phase space and Lorentz structure we are able to describe the data quite well.

D. Calculation of the Lorentz Structure

In this Section, we will calculate the Lorentz structure $|\epsilon_{\mu\nu\alpha\beta} \varepsilon_{\rho'}^\mu \varepsilon_\omega^\nu p^\alpha q^\beta|^2$, where we use p^α and q^β to represent the four momentum of ρ' and ω . In general the helicity structure is more apparent when calculated in a rest frame where the ρ' is in motion. Later we will give the expression in ρ' rest frame.

The transversality $\varepsilon_\omega \cdot p_\omega = 0$ [30]. For spin 1 massive particle with momentum $\vec{p} = p\vec{e}_z$, the helicity states can be represented as:

$$\begin{aligned}\varepsilon_{(\pm)} &= \mp(0, 1, \pm i, 0) \\ \varepsilon_{(0)} &= (p, 0, 0, E)/M\end{aligned}\quad (49)$$

For general \vec{p} , we can construct $\varepsilon_{(0)}$ as follows. The $\varepsilon_{(\pm)}$ are not shown as they will not be directly used.

$$\varepsilon_{(0)} = \left(\frac{p}{M}, \frac{E \vec{p}}{M p} \right) \quad (50)$$

Now we need to prepare calculations of several quantities. First is $\varepsilon_{(\lambda)}^\mu \varepsilon_{(\lambda)}^\nu$. The summation over all helicity states is given in [30]. For helicity 0, we use Eq: 50 and expand it. We have

$$\sum_{\lambda=0,\pm} \varepsilon_{(\lambda)}^\mu \varepsilon_{(\lambda)}^\nu = -g^{\mu\nu} + \frac{p_\mu p_\nu}{M^2} \quad (51)$$

$$\varepsilon_{(0)}^\mu \varepsilon_{(0)}^\nu = \frac{p^\mu p^\nu}{M^2} - \delta_{\mu 0} \delta_{\nu 0} + \frac{(p^\mu p^\nu)^*}{P^2} \quad (52)$$

$$\varepsilon_{(+)}^\mu \varepsilon_{(+)}^\nu + \varepsilon_{(-)}^\mu \varepsilon_{(-)}^\nu = -g^{\mu\nu} + \delta_{\mu 0} \delta_{\nu 0} - \frac{(p^\mu p^\nu)^*}{P^2} \quad (53)$$

In $(p^\mu p^\nu)^*$, only $\mu, \nu = 1, 2, 3$ have non-zero values. In the later calculations, we always assume that transverse helicity states ($\lambda = \pm 1$) have the same probabilities.

For terms like $\epsilon_{\alpha\beta\gamma\delta} p^\alpha p^\beta \dots$, exchanging α and β will introduce a negative sign. Thus the value is zero.

$$\epsilon_{\alpha\beta\gamma\delta} p^\alpha p^\beta \times \text{anything} = 0 \quad (54)$$

The Lorentz structure will be calculated with summation of all helicity states and different polarizations.

$$A_{tot} = A_{00} + A_{01} + A_{10} + A_{11} = \epsilon_{\alpha\beta\gamma\delta} \epsilon_{\kappa\lambda\mu\nu} (\varepsilon^\alpha \varepsilon^\kappa p^\beta p^\lambda)_{\rho'} (\varepsilon^\gamma \varepsilon^\mu q^\delta p^\nu)_\omega \quad (55)$$

where A_{01} for longitudinal polarized ρ' and transverse polarized ω . Others are similar.

There is one term which often shows up; expanding we find:

$$\begin{aligned}\epsilon_{0ijk} \epsilon_{0imn} p_j p_m q_k q_n &= p_2^2 q_3^2 + p_3^2 q_2^2 - 2p_2 p_3 q_2 q_3 \quad (i = 1) \\ &+ p_1^2 q_3^2 + p_3^2 q_1^2 - 2p_1 p_3 q_1 q_3 \quad (i = 2) \\ &+ p_1^2 q_2^2 + p_2^2 q_1^2 - 2p_1 p_2 q_1 q_2 \quad (i = 3) \\ &+ (p_1^2 q_1^2 + p_2^2 q_2^2 + p_3^2 q_3^2) - (p_1^2 q_1^2 + p_2^2 q_2^2 + p_3^2 q_3^2) \\ &= (p_1^2 + p_2^2 + p_3^2)(q_1^2 + q_2^2 + q_3^2) - (p_1 q_1 + p_2 q_2 + p_3 q_3)^2 \\ &= p^2 q^2 - (\vec{p} \cdot \vec{q})^2 = p^2 q^2 (1 - \cos^2 \theta)\end{aligned}\quad (56)$$

Now the summation over all helicity states:

$$\begin{aligned}
A_{tot} &= \epsilon_{\alpha\beta\gamma\delta} \epsilon_{\kappa\lambda\mu\nu} \left(-g^{\alpha\kappa} + \frac{p^\alpha p^\kappa}{M^2} \right) p^\beta p^\lambda \left(-g^{\gamma\mu} + \frac{q^\gamma q^\mu}{m^2} \right) q^\delta q^\nu \quad (57) \\
&= \epsilon_{\alpha\beta\gamma\delta} \epsilon_{\kappa\lambda\mu\nu} g^{\alpha\kappa} g^{\gamma\mu} p^\beta p^\lambda q^\delta q^\nu \\
&= -2\epsilon_{0\beta\mu\delta} \epsilon_{0\lambda\mu\nu} p^\beta p^\lambda q^\delta q^\nu \quad (\alpha = 0 \text{ or } \kappa = 0) \\
&\quad + \epsilon_{\alpha 0\mu\delta} \epsilon_{\alpha 0\mu\nu} p^0 p^0 q^\delta q^\nu \quad (\beta = \lambda = 0) \\
&\quad + \epsilon_{\alpha\beta\nu 0} \epsilon_{\alpha\lambda\mu 0} p^\beta p^\lambda q^0 q^0 \quad (\delta = \nu = 0) \\
&\quad + 2\epsilon_{\alpha 0\mu\delta} \epsilon_{\alpha\lambda\mu 0} p^0 p^\lambda q^\delta q^0 \quad (\beta = \nu = 0 \text{ or } \lambda = \delta = 0) \\
&= -2p^2 q^2 (1 - \cos^2\theta) + 2E_{\rho'}^2 q^2 + 2E_\omega^2 p^2 - 4E_{\rho'} E_\omega p q \cos\theta
\end{aligned}$$

Lorentz structures for longitudinal polarized ρ' and ω :

$$\begin{aligned}
A_{00} &= \epsilon_{\alpha\beta\gamma\delta} \epsilon_{\kappa\lambda\mu\nu} \left(\frac{p^\alpha p^\kappa}{M^2} - \delta_{\alpha 0} \delta_{\kappa 0} + \frac{(p^\alpha p^\kappa)^*}{p^2} \right) p^\beta p^\lambda \left(\frac{q^\gamma q^\mu}{m^2} - \delta_{\gamma 0} \delta_{\mu 0} + \frac{(q^\gamma q^\mu)^*}{q^2} \right) q^\delta q^\nu \quad (58) \\
&= \epsilon_{\alpha\beta\gamma\delta} \epsilon_{\kappa\lambda\mu\nu} (p^\alpha p^\kappa)^* p^\beta p^\lambda (q^\gamma q^\mu)^* q^\delta q^\nu \frac{1}{p^2 q^2} \\
&= 0
\end{aligned}$$

In the first step, only one of nine terms survive; seven terms are eliminated due to Eq. 54. The one which has four δ 's results in two 0 subscripts in each ϵ . In the second step, Eq. 54 limits that β, λ, δ and ν are all zero, which also gives zero.

The Lorentz structures for longitudinal polarized ρ' and transverse polarized ω are:

$$\begin{aligned}
A_{01} &= \epsilon_{\alpha\beta\gamma\delta} \epsilon_{\kappa\lambda\mu\nu} \left(\frac{p^\alpha p^\kappa}{M^2} - \delta_{\alpha 0} \delta_{\kappa 0} + \frac{(p^\alpha p^\kappa)^*}{p^2} \right) p^\beta p^\lambda \left(-g^{\gamma\mu} + \delta_{\gamma 0} \delta_{\mu 0} - \frac{(q^\gamma q^\mu)^*}{q^2} \right) q^\delta q^\nu \quad (59) \\
&= \epsilon_{\alpha\beta\gamma\delta} \epsilon_{\kappa\lambda\mu\nu} \delta_{\alpha 0} \delta_{\kappa 0} g^{\gamma\mu} p^\beta p^\lambda q^\delta q^\nu - \epsilon_{\alpha\beta\gamma\delta} \epsilon_{\kappa\lambda\mu\nu} g^{\gamma\mu} \frac{(p^\alpha p^\kappa)^*}{p^2} p^\beta p^\lambda q^\delta q^\nu \\
&= -\epsilon_{0\beta\mu\delta} \epsilon_{0\lambda\mu\nu} p^\beta p^\lambda q^\delta q^\nu + \epsilon_{\alpha 0\mu\delta} \epsilon_{\kappa 0\mu\nu} \frac{(p^\alpha p^\kappa)^*}{p^2} p^0 p^0 q^\delta q^\nu \\
&= \left(\frac{p^0 p^0}{p^2} - 1 \right) p^2 q^2 (1 - \cos^2\theta) \\
&= M_{\rho'}^2 q^2 (1 - \cos^2\theta) .
\end{aligned}$$

Similarly, Lorentz structures for transverse polarized ρ' and longitudinal polarized ω are:

$$A_{10} = m_\omega^2 p^2 (1 - \cos^2\theta) , \quad (60)$$

while Lorentz structures for transverse polarized ρ' and ω are given by:

$$\begin{aligned}
A_{11} &= A_{tot} - A_{00} - A_{01} - A_{10} \\
&= 2E_{\rho'}^2 q^2 + 2E_\omega^2 p^2 - 4E_{\rho'} E_\omega p q \cos\theta - (2p^2 q^2 + M_{\rho'}^2 q^2 + m_\omega^2 p^2) (1 - \cos^2\theta) \\
&= (E_{\rho'}^2 + E_\omega^2 p^2) (1 + \cos^2\theta) - 4E_{\rho'} E_\omega p q \cos\theta . \quad (61)
\end{aligned}$$

In the rest frame of ρ' , the Lorentz structures are expressed as:

$$\begin{aligned}
A_{tot} &= 2M_{\rho'}^2 q_{\omega}^2 & (62) \\
A_{00} &= 0 \\
A_{01} &= M_{\rho'}^2 q_{\omega}^2 (1 - \cos^2\theta) \\
A_{10} &= 0 \\
A_{11} &= M_{\rho'}^2 q_{\omega}^2 (1 + \cos^2\theta) .
\end{aligned}$$

(Note, that there is no contribution from longitudinal polarized ω .)